Rab7-harboring vesicles are carriers of the transferrin receptor through the biosynthetic secretory pathway

Maika S Deffieu, Ieva Cesonyte, François Delalande, Gaëlle Boncompain, Cristina Dorobantu, Eli Song, Vincent Lucansky, Aurélie Hirschler, Sarah Cianférani, Franck Perez, et al.

CELL BIOLOGY

Rab7-harboring vesicles are carriers of the transferrin receptor through the biosynthetic secretory pathway

Maika S. Deffieu[1,2]*, Ieva Cesonyte[2†], François Delalande[3], Gaelle Boncompain[4], Cristina Dorobantu[2‡], Eli Song[5], Vincent Lucansky[2§], Aurélie Hirschler[3], Sarah Cianferani[3], Franck Perez[4], Christine Carapito[3], Raphael Gaudin[1,2]*

The biosynthetic secretory pathway is particularly challenging to investigate as it is underrepresented compared to the abundance of the other intracellular trafficking routes. Here, we combined the retention using selective hook (RUSH) to a CRISPR-Cas9 gene editing approach (eRUSH) and identified Rab7-harboring vesicles as an important intermediate compartment of the Golgi–to–plasma membrane transport of neosynthesized transferrin receptor (TfR). These vesicles did not exhibit degradative properties and were not associated to Rab6A-harboring vesicles. Rab7A was transiently associated to neosynthetic TfR-containing post–Golgi vesicles but dissociated before fusion with the plasma membrane. Together, our study reveals a role for Rab7 in the biosynthetic secretory pathway of the TfR, highlighting the diversity of the secretory vesicles' nature.

INTRODUCTION

Cells sense environmental changes and adapt accordingly by exposing a variety of transmembrane receptors at their cell surface. Posttranslational modifications and final localization of these transmembrane receptors at the plasma membrane (PM) are first occurring through the membrane dynamics along the secretory pathway. The secretory pathway is a constitutive or regulated process (*1*) carrying neosynthesized proteins from the endoplasmic reticulum (ER) to the PM. Characterizing the molecular mechanisms involved in this cellular process may be useful for the development of inhibitors targeting general or cargo-specific secretion (*2*).

Transmembrane receptors are synthesized and folded in the ER. After synthesis, coatomer protein complex II (COPII) vesicles export the incorporated receptors to the cis-Golgi cisternae (*3*). The transit of these cargoes through the Golgi stacks is still debated (*4*, *5*), although it is well established that proteins undergo successive posttranslational modifications during their trafficking from the cis-Golgi to the trans-Golgi network (TGN). Upon protein arrival at the TGN, cargoes are specifically packaged and sorted to be delivered to different organelles such as endosomes, lysosomes, or the PM. Sorting signals identified at the cytosolic regions of transmembrane receptors lead to the specific recruitment of adaptor proteins or small Rab guanosine triphosphatases (GTPases), needed for the incorporation of the cargo inside vesicle carriers. After budding off the TGN membranes, proteins are delivered to their final destination through vesicular transport. It was long thought that transmembrane receptors use a direct route from the TGN to the PM. Observations of differential trafficking routes suggested otherwise. Several studies noticed the presence of cargoes inside endocytic compartments before their delivery to the PM (*6*–*8*). In particular, Rab11-positive recycling endosomes have been proposed to be involved in the biosynthetic pathway (*7*, *9*), but overall, the nature and fate of these intermediate compartments in protein secretion are still unclear.

To mechanistically understand temporally and spatially the secretory pathway, a few systems were developed. One of the earliest methods developed to study protein secretion was the thermosensitive vesicular stomatitis virus glycoprotein (ts045VSV-G) (*10*). It involves incubation of cells at a restrictive temperature to block ts045VSV-G transport at the ER followed by a shift at a lower permissive temperature to induce the release of the protein to its normal trafficking pathway (*11*). This method provided valuable analytical information on the dynamics and kinetics of transport of ts045VSV-G from the TGN to the PM.

To avoid nonphysiological conditions of temperature and monitor different cargo proteins, the RUSH (retention using selective hooks) system was elaborated (*12*). It allows the retention of a protein of interest in the ER and then its on-demand release following the addition of biotin in the cell media. This method proved to be very powerful (*2*, *13*–*16*), but it requires the transient overexpression of the protein of interest, which is a limitation in case of regulated secretion. In addition, the coexistence of the overexpressed tagged and nontagged endogenous cargos could confer some limitations for quantitative temporal detection of a receptor at the PM.

The vesicular carriers involved in the secretory pathway are difficult to study because of their low abundance at steady state compared to endocytic/recycling vesicles. This is particularly true for transferrin receptor 1 (TfR), which is widely used for recycling studies [for review, see (*17*)]. TfR is a ubiquitous transmembrane glycoprotein that mediates iron uptake from circulating transferrin (Tf) at the PM. After formation of the TfR-Tf complex at the cell surface, the receptor is internalized by clathrin-mediated endocytosis and delivered to endosomes. Inside these organelles, TfR dissociates from its ligand and is recycled back to the cell surface. Studies indicated that an alteration of the expression level of TfR could trigger carcinoma

[1]Institut de Recherche en Infectiologie de Montpellier (IRIM) CNRS, Univ Montpellier, 34293 Montpellier, France. [2]INSERM, Univ Strasbourg, 67000 Strasbourg, France. [3]Laboratoire de Spectrométrie de Masse Bio-Organique, IPHC, UMR 7178, CNRS-Université de Strasbourg, ECPM, 67087 Strasbourg, France. [4]Institut Curie, PSL Research University, Sorbonne Université, Centre National de la Recherche Scientifique, UMR 144, 26 rue d'Ulm, F-75005 Paris, France. [5]National Laboratory of Biomacromolecules, Institute of Biophysics, Chinese Academy of Sciences, Beijing 100101, China.
*Corresponding author. Email: raphael.gaudin@irim.cnrs.fr (R.G.); maika.deffieu@irim.cnrs.fr (M.S.D.)
†Present address: Virology Section, Infectious Diseases and Immunology Division, Department of Biomolecular Health Sciences, Faculty of Veterinary Medicine, Utrecht University, Utrecht, Netherlands.
‡Present address: Janssen Vaccines & Prevention B.V., Newtonweg 1, 2333CP Leiden, Netherlands.
§Present address: Comenius University in Bratislava, Jessenius Faculty of Medicine in Martin (JFMED CU), Biomedical Center Martin, Mala Hora 4C, 036 01 Martin, Slovakia.

progression (*18*, *19*). Cancer cells expressed a high amount of TfR at their cell surface, which makes it a notable anticancer target (*20*, *21*).

Neosynthesized TfR arriving at the PM represents a minor fraction of the total TfR pool expressed at the cell surface at steady state, and thus, the pathway of newly synthesized TfR is particularly difficult to investigate. In this study, we developed an approach that combines the RUSH system with CRISPR-Cas9 gene editing that we called "edited-RUSH" or "eRUSH." We used eRUSH to investigate the molecular mechanisms involved in the vesicular transport of neosynthesized TfR to the PM. TfR-eRUSH allowed the spatiotemporal monitoring of the trafficking of the neosynthesized endogenous TfR and the identification of the molecular partners involved in this process. In particular, we highlighted that Rab7A, a small Rab GTPase usually described as an endolysosomal marker, is required for efficient arrival of neosynthesized TfR at the PM and was recruited to a subset of post-TGN TfR-containing vesicles, suggesting that Rab7 may play a role in the anterograde trafficking pathway of secretory vesicles.

RESULTS

Generation and characterization of the TfR-eRUSH system

The CRISPR-Cas9 strategy that we previously described (*22*) was used to engineer the breast cancer–derived SUM159 cells to express endogenous TfR fused to the streptavidin-binding peptide (SBP) and enhanced green fluorescent protein (EGFP). Lentiviral transduction of a chimera streptavidin-KDEL protein was performed to establish a stable cell line that retains proteins expressing the SBP motif in the luminal side of the ER [see (*12*) for the original description of the RUSH system], and the resulting TfR-eRUSH cells were subsequently characterized.

As depicted in Fig. 1A, SBP fused to EGFP was introduced in the genomic sequence of TfR before its stop codon sequence. At the genomic DNA level, both alleles were carrying an extra piece of DNA corresponding to the SBP-EGFP tag (Fig. 1B). At the protein level, almost no endogenous TfR was detected (at ≈84 kDa), while an upper band at ≈117 kDa appeared, corresponding to the expected size of TfR-SBP-EGFP protein (fig. S1A). Notably, the molecular weights were difficult to precisely assess as ladders from different brands were providing dissimilar sizes for a given band. Using an anti-EGFP antibody, we could confirm that TfR-SBP-EGFP was running at an apparent size of 117 kDa (fig. S1B). Depending on the ladder used along our study, TfR-eRUSH would appear as a band of either ≈98 or 117 kDa, although both would correspond to TfR-eRUSH.

From the immunoblot, it seemed that less TfR-SBP-EGFP proteins were expressed in the edited cells than the endogenous TfR from wild-type (WT) cells. However, quantification of the amount of proteins from bands of different sizes is not reliable because of different protein transfer efficiency. Thus, an anti-TfR antibody staining on WT and TfR-eRUSH cells was performed, and the mean fluorescence intensity (MFI) of the TfR staining was measured by flow cytometry. We found that TfR-eRUSH cells express less endogenous TfR than their parental cell line (Fig. 1C).

Next, we carried out three-dimensional confocal live-cell imaging on TfR-eRUSH cells to determine whether TfR-eRUSH could be efficiently retained in the ER. We observed that in the absence of biotin (0 min), TfR-eRUSH was retained in the ER (Fig. 1D, top, and corresponding movie S1). Two to 6 min after biotin addition, vesicles were released from the ER to reach the Golgi apparatus. This trend was successfully quantified by measuring the Pearson's correlation coefficient between TfR and either calnexin (ER marker), GM130 (cis-Golgi), or TGN46 (trans-Golgi) at 0, 5, and 15 min after biotin addition (fig. S1, C and D). While the ER released most of its vesicles, a short lag was observed at ≈12 min before observing numerous vesicles exiting from the Golgi apparatus. At 20 min, most of TfR-eRUSH was localized at the Golgi, and vesicles were massively released from this location. In parallel, PM gained higher TfR-eRUSH fluorescence intensity (Fig. 1D, blue arrowheads, and movie S1), indicating that the first detectable amounts of TfR-eRUSH proteins arrived at the PM at 20 min after biotin addition.

To quantitatively measure the kinetics of TfR-eRUSH arrival at the PM, a flow cytometry assay was optimized (Fig. 1E). At different times after biotin addition, cells were incubated at 4°C to block membrane trafficking and the PM-exposed TfR was labeled using recombinant transferrin coupled to an Alexa Fluor 647 (Tf-A647) (Fig. 1E). We noticed that a small fraction of TfR-eRUSH was already found at the PM even in the absence of biotin (0 min), suggesting either that some aspecific Tf binding occurred or that a small amount of TfR-eRUSH was not retained by the hook. While the fluorescence signal of Tf-A647 was lowly increasing over the first 20 min after biotin addition, a threefold increase was observed at 30 min after biotin addition. This kinetics was confirmed by microscopy (Fig. 1F) and is in agreement with our live-cell imaging (Fig. 1D), in which the first TfR proteins could be readily detected at the PM at ≈23 min after biotin addition, then rising over time. In conclusion, our TfR-eRUSH system represents a valid approach to study the molecular mechanism of the TfR secretory pathway in an endogenous synchronized model.

Molecular signature of the TfR-associated membranes using TfR-eRUSH cells

To identify the molecular partners enriched in the TfR-containing membranes over time, anti-TfR affinity purification mass spectrometry (AP-LC-MS/MS) experiments using TfR-eRUSH lysates obtained from mechanical cell disruption were performed at different time points after biotin addition. AP-LC-MS/MS was run in quadruplicate, and >2000 proteins were identified in each sample. Differential temporal analysis identified 557 proteins enriched at T15 compared to T0 (T0-T15), while no significant protein enrichment could be measured at T30 compared to T15 (T15-T30). This absence of protein enrichment between T15 and T30 could be attributed to the lack of temporal resolution and/or the fact that multiple trafficking pathways are overlapping at these times, blurring the final picture. Parallel analyses using STRING (*23*) (Fig. 2A) and the molecular signature database MSigDB (*24*) (Fig. 2B and table S1) were run on the enriched protein lists from the T0-15 differential analysis. These methods were used to highlight protein clusters and biological processes associated to neosynthesized TfR trafficking.

The pathways "intracellular transport," "cellular macromolecular localization," "intracellular protein transport," and "secretion" were highly enriched compared to T0 as shown by the low false discovery rate (FDR) values, an expected result due to the nature of the assay (Fig. 2B). Moreover, the pathways associated to "exocytosis" (FDR = 4.75×10^{-23}) and "Golgi vesicle transport" (FDR = 2×10^{-15}) were also significantly enriched to a lower extent. As a proof of concept, we confirmed that TMED10, a protein identified as enriched in our proteomics analyses, was recruited to TfR secretory vesicles (table S1 and fig. S2A). TMED10 is involved in the COPII vesicle–mediated

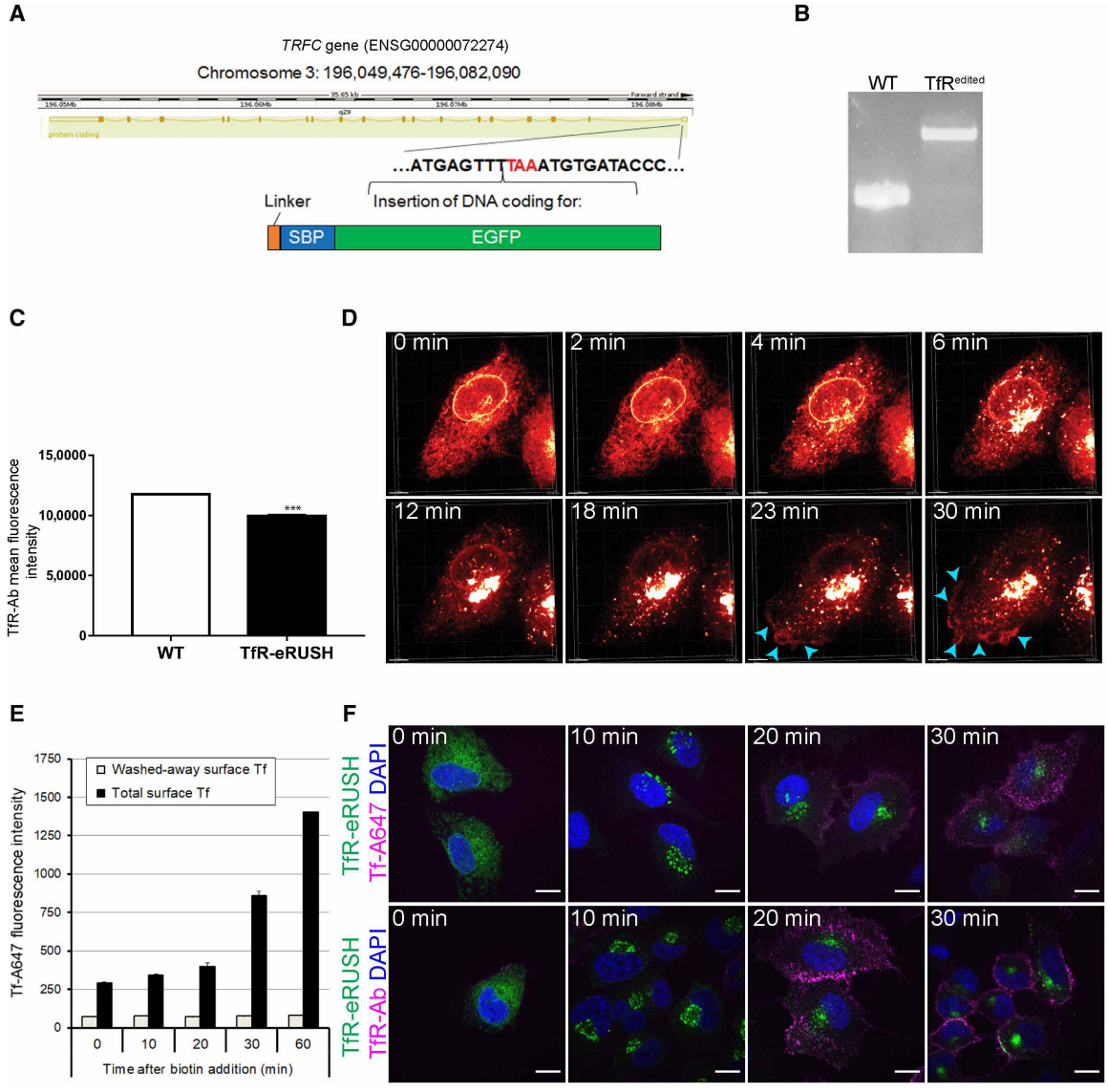

Fig. 1. Generation and characterization of TfR-eRUSH gene-edited cells. (**A**) Scheme illustrating the insertion of the linker-SBP-EGFP coding sequence in the chromosomal region containing the stop codon (red) of the *TFRC* gene (transferrin receptor type 1, referred to as TfR). (**B**) PCR amplification from genomic DNA using primers flanking the TfR stop codon region confirmed the insertion of the SBP-EGFP sequence on both alleles. (**C**) Flow cytometry analysis indicates the total amount of TfR expressed in wild-type (WT) and TfR-eRUSH cells. MFI is represented ± SD (10,000 cells per condition, $n = 3$ independent experiments performed in duplicate). Student's t test (***$P < 0.001$). (**D**) Representative live-cell imaging of TfR-eRUSH cells showing protein distribution after biotin addition. Note that TfR-eRUSH is at the PM starting from 23 min after biotin addition (blue arrowheads). (**E**) Flow cytometry analysis representing the amount of Tf-A647 bound at the surface of TfR-eRUSH cells. Note the increase of Tf fluorescence starting from 20 min after biotin addition. MFI is represented ± SD (5000 cells per condition, $n = 3$ individual experiment performed in duplicate). (**F**) Representative confocal immunofluorescence images detecting the arrival of TfR-eRUSH at the PM. TfR-eRUSH (green), Tf-A647 (magenta, top), or anti-TfR antibody (TfR-Ab, bottom) was detected at the PM starting from 20 min after biotin addition. Scale bars, 10 μm.

anterograde transport (*25*) and incorporated in a subset of extracellular vesicles (*26*), and thus, we could confirm the relevance of our differential proteomics approach.

The pathways "oxidation reduction process," "cellular respiration," and "mitochondrion organization" also scored significantly low FDR values. ER and mitochondrial membranes are well known to tightly interact (*27*), and recent work proposed that endosome-mitochondria interactions are important for the release of iron (*28*). Here, the mitochondria-associated proteins identified may be the result of association of distinct membranes during the immunoprecipitation rather than the actual presence of TfR within mitochondria. Proximity was observed between TfR-eRUSH and MitoTracker-labeled mitochondria (fig. S2B). By live-cell imaging, we visualized some rare events of mitochondria "associated" with vesicles containing TfR-eRUSH that seemed to bud off the ER, but the resolution achieved with our spinning disk confocal microscope does not allow us to draw a significant conclusion (fig. S2C and movie S2).

Proteins regulating intracellular trafficking may be differentially recruited on vesicular membranes to activate a specific trafficking route. Therefore, we chose to further investigate the role of Rab

A

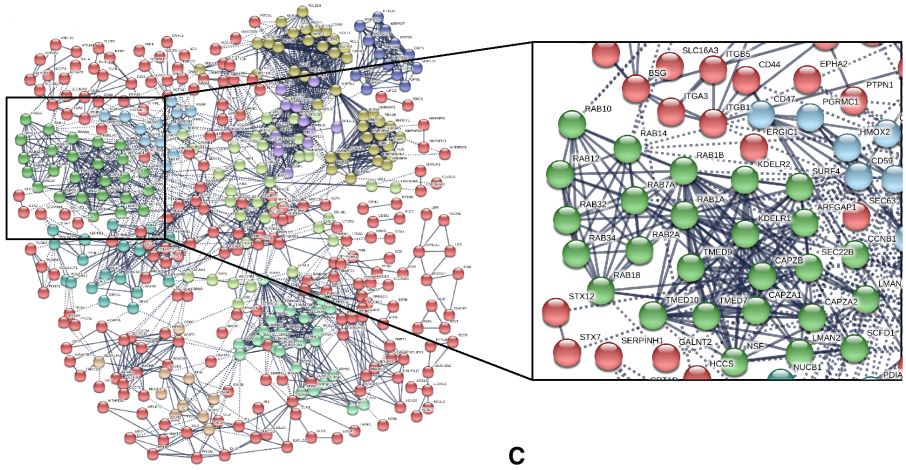

B

Pathway (biological process)	FDR *q* value
Oxidation reduction process	5.61×10^{-71}
Intracellular transport	8.01×10^{-51}
Organic acid metabolic process	2.70×10^{-45}
Cellular macromolecule localization	4.77×10^{-37}
Cellular respiration	1.79×10^{-36}
Intracellular protein transport	3.67×10^{-34}
Response to endoplasmic reticulum stress	1.08×10^{-29}
Lipid metabolic process	3.61×10^{-29}
Mitochondrion organization	1.36×10^{-27}
Secretion	3.69×10^{-26}

C

Protein	Fold enrichment	*P* value
RAB18	1.89	0.0021
RAB32	1.82	0.0026
RAB7A	1.73	0.0080
RAB10	1.70	0.0071
RAB2A;RAB2B	1.70	0.0102
RAB1B	1.64	0.0233
RAB14	1.61	0.0093
RAB1A	1.60	0.0053
RAB34	1.54	0.0183
RAB12	1.52	0.0113

D

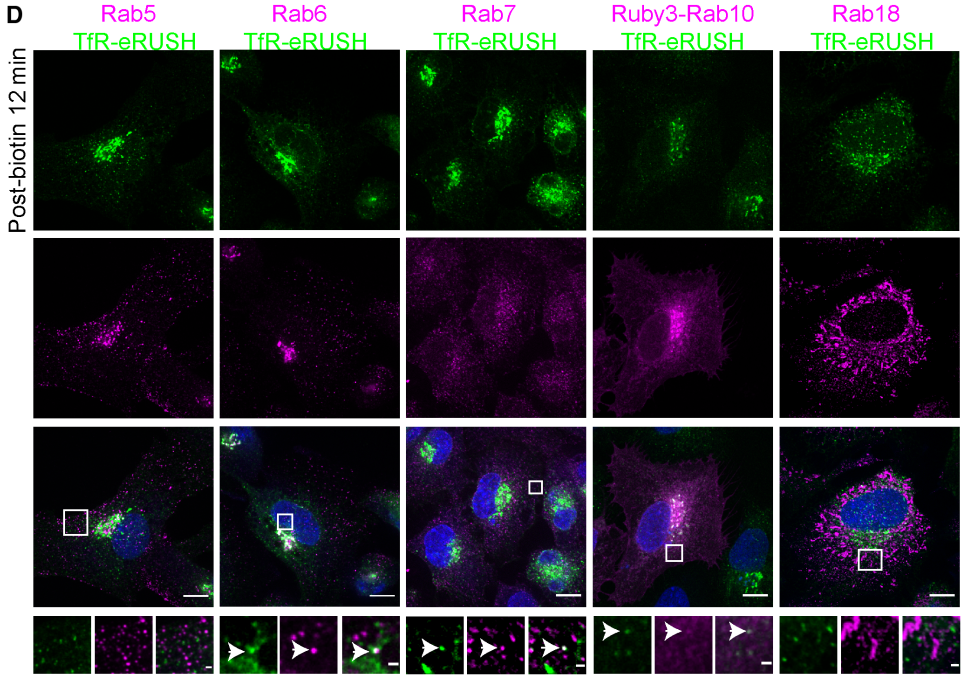

Fig. 2. Proteomics analysis of neosynthesized TfR-containing membranes. (**A** to **C**) LC-MS/MS proteomics analysis of immunoprecipitated TfR-eRUSH following biotin addition. (A) STRING analysis shows the interaction map of proteins that were enriched at T15 compared to T0. Color codes highlight clusters of proteins of related functions. (B) GO of the proteins enriched at least 1.5 times with a significant *P* value (<0.05) at T15 compared to T0 (T0-T15) was investigated using the GSEA online software. Relevant GO pathways and their corresponding FDR values are reported for each differential analysis. (C) The table reports the fold enrichment and *P* values of the Rab proteins significantly enriched at T15 compared to T0 (see table S2). (**D**) Representative confocal images from a single z-stack indicate the distribution of TfR-eRUSH treated for 12 min with biotin relative to the endogenous Rab5, Rab6, Rab7, and Rab18 proteins and the exogenously expressed Ruby3-Rab10. Note that TfR-eRUSH co-distributes in vesicles containing Rab7, Rab6, or Ruby3-Rab10 (zoomed panels, white arrowheads). Scale bars, 10 μm. Zoomed regions from white squares are represented with scale bars of 1 μm.

proteins as they are well-known small GTPase regulators of intracellular membrane traffic. In our AP-LC-MS/MS dataset, we detected a total of 20 Rab proteins (table S2). No Rab proteins were enriched in TfR-containing membranes at T15-T30, but 10 Rab proteins were significantly enriched at T0-T15 with a fold change above 1.5 times (Fig. 2C). Rab1A, Rab1B, and Rab18 were significantly enriched at T15 compared to T0, an expected result as these Rabs regulate vesicle trafficking between the ER and the cis-Golgi (*29*, *30*), Rab18 being also found on a subset of extracellular vesicles (*26*). Rab10, Rab14, and Rab6A were also enriched at T15 compared to T0, although Rab6 did not reach significance (table S2). These Rabs have previously been involved in post-Golgi trafficking (*14*, *31*, *32*), further indicating that our approach is relevant to identify molecular partners involved in the secretory pathway. The Rab12 and Rab34 proteins were also identified, but their function has not been extensively studied. However, they both may play a role in protein degradation (*33*, *34*). Last, Rab7A, a protein usually recruited at the limiting membrane of late endosomes that can serve as degradation signal (*35*), was significantly enriched at T15 compared to T0. Rab7A showed one of the highest fold enrichment scores and the greatest number of unique peptides identified by LC-MS/MS (Fig. 2C and table S2), an intriguing result that we aimed to explore thereafter.

To correlate our proteomics analyses to the actual co-distribution of TfR and Rabs, TfR-eRUSH cells treated for 12 min with biotin and the presence/absence of Rab5, Rab6, Rab7, Ruby3-Rab10, and Rab18 were assessed (Fig. 2D). While no colocalization could be seen between TfR-eRUSH and Rab5 and Rab18, a subset of the Rab6, Rab7, and Rab10 signal was colocalizing with TfR-eRUSH. These qualitative observations complement the proteomics analyses in Fig. 2C and highlight Rab7 as an interesting unexpected partner involved in the biosynthetic secretory pathway.

Rab7 is significantly enriched onto post-Golgi TfR-eRUSH vesicles

To further characterize the recruitment of Rab7A on TfR-containing secretory vesicles, we performed live-cell imaging by spinning disk confocal microscopy on TfR-eRUSH cells transfected with a Ruby3-Rab7A construct under the control of the weak promoter L30 (to minimize overexpression). Starting from 7 min after biotin addition, we noticed the presence of post-TGN TfR-eRUSH signal associated to Rab7A-positive vesicles (Fig. 3A and movie S3). To better appreciate whether TfR-eRUSH and Rab7A were found on the same vesicles (as opposed to two distinct vesicles in close proximity), we artificially swelled these compartments using apilimod, a PIKfyve inhibitor (*36*), and we could identify that TfR-eRUSH–positive vesicles were decorated with Rab7A at their limiting membrane (Fig. 3B). These data were reminiscent of a recent work nicely demonstrating that post-Golgi vesicles were positive for Rab6 (*14*), and in our model, TfR-eRUSH was also trafficking through Rab6 (fig. S3A).

Quantification of TfR-eRUSH association with indicated Rabs was then performed using antibody staining on TfR-eRUSH cells fixed at 15 min after biotin addition. As expected, the percentage of non-Golgi TfR-eRUSH signal associated to Rab5 was very low (9.3 ± 1.3%), while association with Rab6 and Rab7 was relatively high (31.7 ± 2.5% and 42.3 ± 3.3%, respectively; Fig. 3, C and D). However, TfR-eRUSH vesicles would harbor either Rab7A or Rab6, but no post-Golgi TfR-eRUSH-Rab6-Rab7A triple colocalization was seen (fig. S3B). Together, our proteomics analysis revealed that several Rabs are enriched onto secretory TfR-containing vesicles and that Rab7A represents an unexpected protein recruited in the neosynthetic secretory pathway.

Neosynthesized TfR associates with nondegradative Rab7 vesicles

Rab7 is known to direct late endosomal compartments toward degradative Lamp1-positive compartments (*37*). By immunostaining, we observed that a subset of TfR-eRUSH was Rab7 positive and Lamp1 negative (Fig. 4A, yellow arrowheads), but we could also see triple colocalization of TfR-eRUSH, Rab7, and Lamp1 (Fig. 4A, white arrowheads). However, mapping the association with Lamp1 is not sufficient to define lysosomal compartments because a recent study demonstrated that TfR is co-sorted with Lamp1 into post-TGN secretory vesicles en route to the PM (*16*). Moreover, Lamp1 was also identified in our proteomics analysis (table S1).

Therefore, to better address whether the TfR-Rab7 vesicles correspond to degradative compartments, pH acidity and proteolytic activity were measured (Fig. 4, B and C). TfR-eRUSH cells were transfected with Ruby3-Rab7A and visualized by live imaging at 10 min after biotin addition. LysoTracker was used as a readout for relative pH acidity (a brighter signal corresponding to a lower pH). Our data show that TfR-eRUSH vesicles harboring Rab7A had little to no LysoTracker signal (Fig. 4B, white arrows), indicating that these vesicles do not exhibit features of classical proteolytic compartments. To assess for actual degradative properties of these vesicles, we preincubated the cells with DQ-BSA, a bovine serum albumin (BSA) protein that contains self-quenched fluorescent dyes that fluoresce only when the BSA is cleaved, and stained the cells with an anti-Rab7 antibody (Fig. 4C). Quantification of the percentage of TfR-eRUSH colocalizing with Rab7 or DQ-BSA demonstrated that the TfRs were mainly found in Rab7 vesicles devoid of degraded DQ-BSA (Fig. 4D). Last, we checked whether TfR-eRUSH was sent for degradation using bafilomycin A1 (Baf A1), a treatment that prevents lysosomal acidification and thus protein degradation as routinely used for autophagy studies (*38*). This treatment provokes the accumulation of quickly degraded protein, as expectedly seen for LC3-II (Fig. 4E). In contrast, however, Baf A1 did not induce an accumulation of TfR-eRUSH, suggesting that it is not sent to the degradation. To make sure that the absence of visible degradation was not due to neosynthesized TfR-eRUSH replenishment, cells were cotreated with Baf A1 and cycloheximide, a translation inhibitor. In this context, we could not observe any accumulation of TfR (Fig. 4E), and we were not able to detect degradation products using either anti-TfR or anti-EGFP antibodies (fig. S4), suggesting that TfR-eRUSH is not significantly sent for degradation. Notably, this experiment also indicates that the induction of eRUSH by the addition of biotin is not accompanied by the induction of autophagy as LC3-II is not up-regulated (Fig. 4E). To further confirm this, LC3 staining was performed, and we could not observe any LC3 staining colocalizing with Rab7-positive TfR-eRUSH vesicles (Fig. 4F, white arrows), indicating that they do not correspond to autophagosomes.

Rab7A vesicles are intermediate compartments mediating the transport of a subset of neosynthesized TfR-eRUSH to the PM

To correlate the enrichment over time of Rab proteins to a biological function, we next carried out a small interfering RNA (siRNA)–based screen targeting 12 members of the Rab protein family. Silencing of 12 Rabs and a nonrelevant target was performed using a pool of four siRNAs per target in two independent experiments (Fig. 5A). The amount of TfR-eRUSH at the PM was measured by flow cytometry

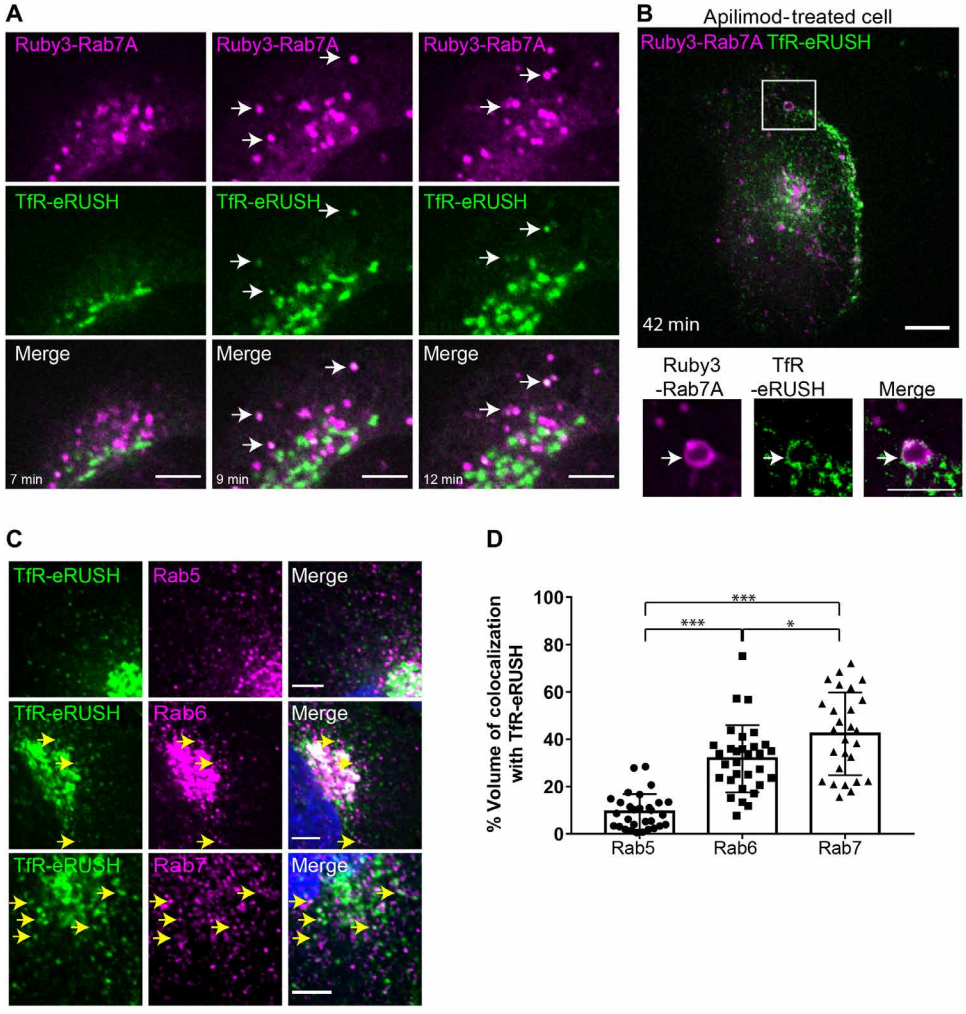

Fig. 3. Identification of Rab7 as an intermediate compartment of neosynthesized TfR trafficking. (**A**) Live-cell imaging shows localization of TfR-eRUSH in Ruby3-Rab7A–transfected cells. Images were extracted from a single plane at 7, 9, and 12 min after biotin addition. Note that TfR-eRUSH (green) co-distributes with Ruby3-Rab7A (magenta)–positive vesicles (white arrows). Scale bars, 5 μm. (**B**) TfR-eRUSH cells expressing Ruby3-Rab7A were imaged after apilimod treatment. Images were extracted as a single plane at 42 min after biotin addition. Scale bar, 10 μm. The zoomed region from the white square highlights that TfR-eRUSH (green) localizes at the limiting membrane of Ruby3-Rab7A vesicles (magenta, white arrows). Scale bar, 5 μm. (**C**) Representative images from a single z-stack indicate the localization of TfR-eRUSH relative to the endogenous Rab5, Rab6, and Rab7. Note that TfR-eRUSH co-distributes with Rab6 or Rab7 (yellow arrows). Scale bars, 5 μm. (**D**) The graph represents the percentage of colocalization between TfR-eRUSH (±SEM) and endogenous Rab5, Rab6, or Rab7 signal. Data represent $n = 30$ cells (Rab5), $n = 31$ cells (Rab6), and $n = 27$ cells (Rab7) per condition from three independent experiments, and Tukey test was run for significance (*$P < 0.05$ and ***$P < 0.001$).

as in Fig. 1E, and fold enrichment of T15 over T0 (Fig. 5A) was determined. As Rabs may affect other cellular processes, the amount of TfR-eRUSH at steady state was measured by flow cytometry (fig. S5A).

At T0-T15, silencing of Rab27A or Rab6A showed a significant decrease of PM-associated TfR (Fig. 5A) compared to the nonrelevant siRNA control. These findings were in agreement with the role of these Rabs in protein secretion (*14*, *39*, *40*), validating our approach. In contrast, Rab10 silencing had no detectable effect on TfR trafficking to the PM, while we found it enriched in our proteomics analysis (Fig. 2C). However, silencing of Rab7A showed a significant inhibition of TfR-eRUSH arrival at the PM (Fig. 5A). These data were confirmed using a single Rab7A-targeting siRNA sequence, while knockdown of RILP (Rab7-interacting lysosomal protein), a Rab7 effector (*41*), had no significant effect on TfR arrival (Fig. 5B). Protein expressions were effectively down-regulated (fig. S5B). Because of the potential off-target effect of siRNA approaches, we overexpressed the dominant negative protein Rab7A T22N (fig. S5C) and showed that it also induced a significant reduction of TfR arrival to the PM (Fig. 5C). Moreover, in experiments using an siRNA-resistant Rab7 construct, we found partial rescue of TfR arrival at the PM (fig. S6). Although the trend was consistent with our previous observations, the differences did not reach significance. This may be explained by the difficulty to control for siRNA-resistant Rab7 protein level, whose overexpression perturbs normal intracellular membrane trafficking (*42*). Although Rab7A is known for its role in endocytic retrograde trafficking to late endosomes and lysosomes (*35*), this is consistent with our AP-LC-MS/MS data (Fig. 2C), further indicating that Rab7 could participate in the transport of post-TGN TfR vesicles.

To directly determine the fate of the Rab-harboring post-Golgi TfR-eRUSH vesicles, total internal reflection fluorescence (TIRF)

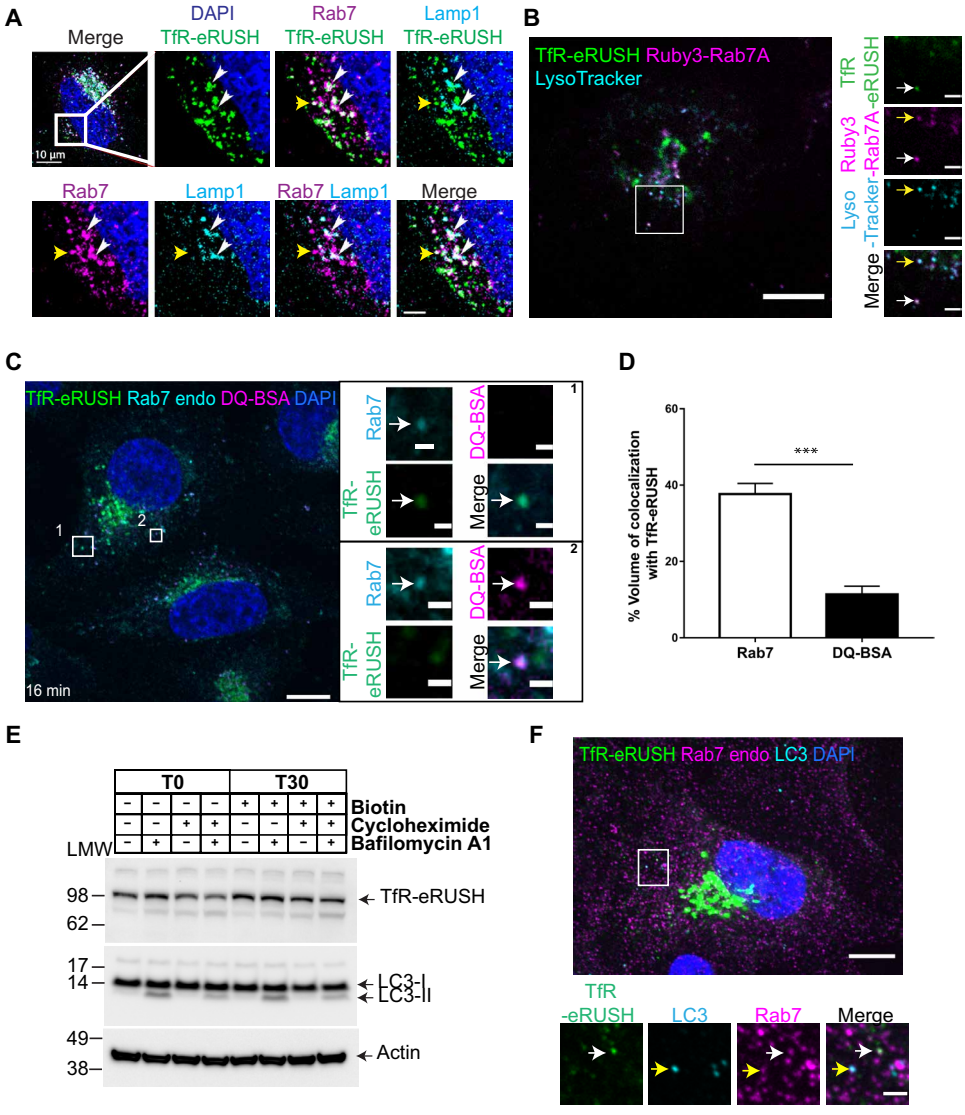

Fig. 4. TfR-eRUSH transiting through Rab7 vesicles localizes at the PM. (**A**) TfR-eRUSH distribution relative to Lamp1 and Rab7$^+$ vesicles. Note that different types of vesicles are observed: TfR-eRUSH vesicles (green) labeled with Rab7 (magenta) and Lamp1 (cyan) (white arrowheads); TfR-eRUSH vesicles labeled with Rab7 but no Lamp1 (yellow arrowheads). Scale bar, 2 µm. (**B**) Live-cell imaging of TfR-eRUSH cells expressing Ruby3-Rab7A in the presence of LysoTracker. At 10 min after biotin addition, note that TfR-eRUSH-Ruby3-Rab7A$^+$ vesicles do not contain LysoTracker (white arrows, zoomed panels) and are distinct from Ruby3-Rab7A$^+$ (magenta) vesicles containing only LysoTracker (cyan, yellow arrows). Scale bars, 2 µm (right) and 10 µm (left). (**C**) Confocal imaging showing TfR-eRUSH and Rab7 localization in the presence of DQ-BSA. Scale bar, 10 µm. At 16 min after biotin addition, TfR-eRUSH vesicles (green) labeled with Rab7 (cyan) do not contain DQ-BSA (square 1, white arrows), while DQ-BSA (magenta) is found only in Rab7$^+$ vesicles (cyan) (square 2, white arrows). Scale bars, 2 µm. (**D**) Quantification of TfR-eRUSH colocalization with Rab7A or DQ-BSA. Data represent the percentage of colocalization with TfR-eRUSH (±SEM) with $n = 32$ cells (DQ-BSA) and $n = 28$ cells (Rab7) from $n = 3$ independent experiments. Student's t test (***$P < 0.001$). (**E**) TfR-eRUSH protein is not degraded upon biotin addition, in the presence of cycloheximide and Baf A1. Actin (loading control), LMW (low molecular weight) marker. Note that the LC3-II bands are more intense in all conditions treated with Baf A1, showing a control for protein degradation. (**F**) Confocal imaging visualizing TfR-eRUSH-Rab7$^+$ vesicle localization relative to LC3. At 15 min after biotin addition, note that TfR-eRUSH (green)-Rab$^+$ (magenta) vesicles do not co-distribute with LC3 (white arrows), although LC3 (cyan) vesicles are labeled with Rab7 (yellow arrows). Scale bars, 2 and 10 µm (top).

microscopy was performed on cells transfected with Ruby3-Rab7A (Fig. 5D and movie S4) or Ruby3-Rab6A (Fig. 5E and movie S5). At 12 min after biotin addition, the arrival of TfR-eRUSH was observed in the evanescent TIRF field. We monitored events during which Rab7-positive vesicles became positive for TfR-eRUSH for several seconds (from 704 to 736 s; Fig. 5D) before the two signals segregated again, followed by a TfR-eRUSH signal burst, indicative of PM fusion (734 s). In sharp contrast, Ruby3-Rab6A remained associated to TfR-eRUSH vesicles until fusion occurred (848 to 868 s; Fig. 5E).

These observations indicate that Rab7A vesicles are used as intermediate compartments in TfR trafficking after its release from the TGN. Unlike Rab6A, Rab7A vesicles do not accompany neosynthesized TfR all the way to the PM, and thus, other partners are likely involved downstream of the Rab7-TfR vesicle trafficking.

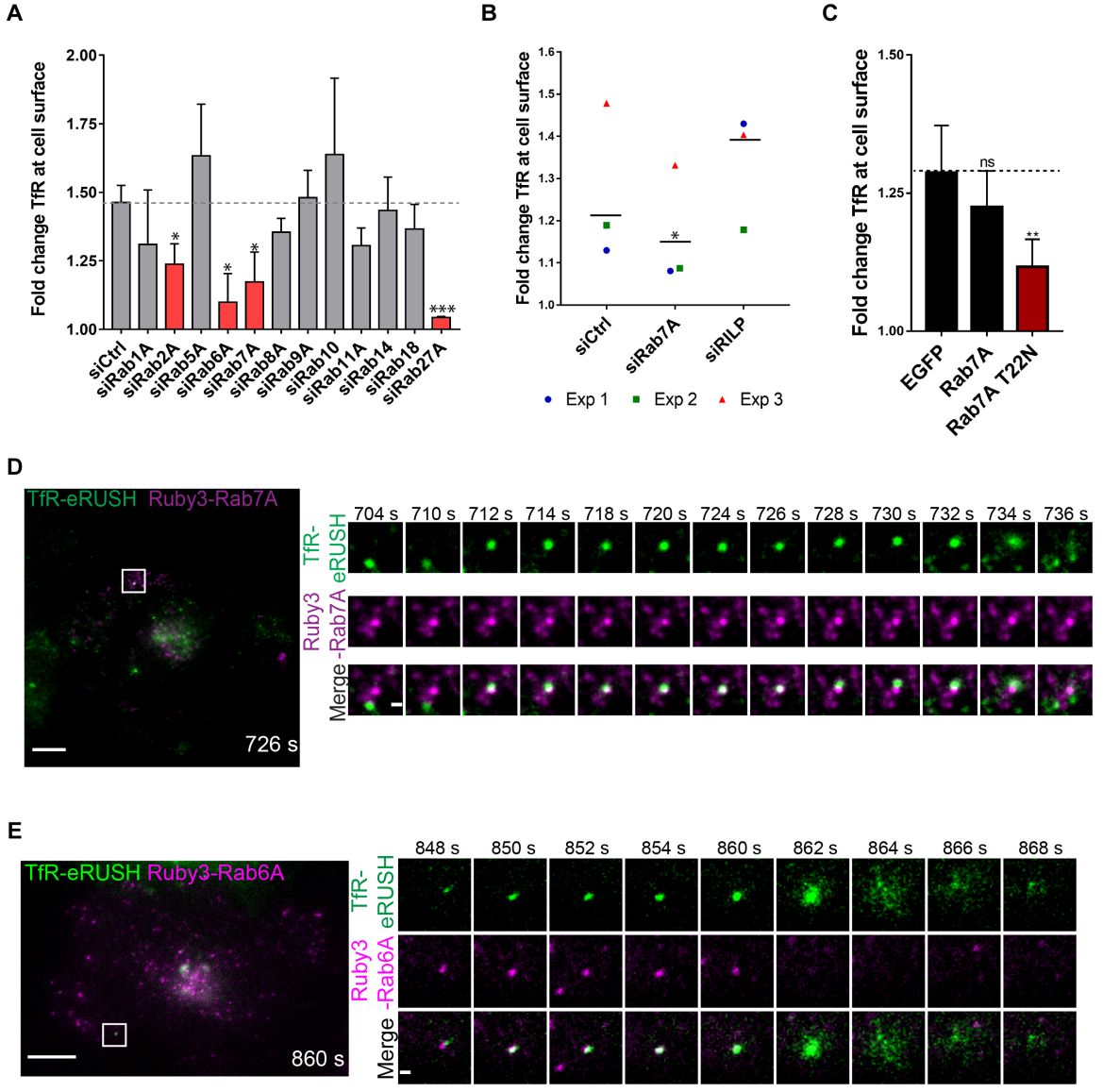

Fig. 5. Rab7A is involved in transport of TfR-eRUSH to the PM. (**A**) Flow cytometry assay measuring the level of TfR-eRUSH at the PM in cells treated with pooled siRNA sequences targeting 12 different Rab mRNAs and a nontargeting siRNA control. The screen was performed in duplicate in $n = 2$ (±SD) independent experiments (2000 cells per condition). Significance was evaluated using ratiometric paired *t* test (*$P < 0.05$; ***$P < 0.0001$). (**B**) Flow cytometry assay measuring the level of TfR-eRUSH at the PM in cells treated with single sequence-specific siRNA targeting Rab7, RILP, or an irrelevant RNA. Each dot represents an independent experiment performed in quadruplicate (10,000 cells analyzed for each condition). The black bars represent the mean of the three experiments. Ratiometric paired *t* test (*$P < 0.05$). (**C**) Flow cytometry assay measuring the level of TfR-eRUSH at the PM in TfR-eRUSH cells expressing EGFP, GFP-Rab7A, or GFP-Rab7A T22N. Data shown are $n = 3$ independent experiments (±SD) (5000 cells per condition), and ratiometric paired *t* test was used for significance (**$P < 0.001$). ns, nonsignificant. (**D**) TfR-eRUSH cells transfected with Ruby3-Rab7A were imaged by TIRF microscopy. A representative image extracted from movie S4 is shown at 726 s. Scale bar, 10 μm. Note that TfR-eRUSH (green) is carried to the PM by Ruby3-Rab7 (magenta) vesicle (cropped regions). Scale bar, 1 μm. (**E**) TfR-eRUSH cells transfected with Ruby3-Rab6A were imaged by TIRF microscopy 24 hours after transfection. A representative image extracted from movie S5 is shown at 860 s. Scale bar, 10 μm. Ruby3-Rab6A (magenta) vesicle carried TfR-eRUSH (green) at the PM (cropped regions). Scale bar, 1 μm.

DISCUSSION

Description of the different pathways mediating transport of neosynthesized receptors to the PM has been studied for decades. Being able to specifically observe the anterograde pathway has always been a challenge as its visualization overlaps with other trafficking routes, including the overrepresented endocytosis and recycling pathways. To visualize protein transport under physiological conditions, we combined the RUSH system to the CRISPR-Cas9 technology. Using TfR as a model, we generated a stable cell line expressing endogenous levels of the receptor fused to EGFP and the SBP tag required for the RUSH system. TfR function and trafficking are well described, but the partners involved in neosynthesized TfR trafficking to the PM are not well characterized. The eRUSH approach was coupled to quantitative proteomics experiments and cytometry-based screening to identify the molecular partners involved in the neosynthetic pathway of the TfR. Unexpectedly, we observed that a significant

subset of TfR transits through Rab7-positive vesicles during its trafficking to the PM.

The trafficking kinetics of neosynthesized TfR-eRUSH was similar to the overexpressed TfR in the RUSH system that was previously described to reach the PM ≈30 min after biotin addition (*16*). The advantage of our eRUSH is that no or minimal amount of "ghost" untagged proteins are expressed in TfR-eRUSH, allowing quantitative single-molecule counting and whole-TfR functional analysis. Moreover, eRUSH also represents a powerful knock-away system, similar to other methods (*43*), but without the problem of competition with the WT version of the protein coexpressed in the cell. In contrast to classic complementary DNA (cDNA) transfection, CRISPR-Cas9–based gene editing of TfR allows the conservation of the regulatory genomic environment of the gene. This parameter is particularly important for proteins such as TfR, as its transcriptional/translational regulation is a finely regulated process (*44*, *45*).

Using AP-LC-MS/MS, we could track the local TfR environment at different times after biotin addition and identify proteins co-distributing with TfR-extracted membranes. Whereas previous siRNA-based screens studying the secretory pathway allowed the identification of previously unidentified partners (*46*), our eRUSH-based proteomics is based on a noninterfering approach, and thus, it provides new complementary information to previous studies. Pathway analysis revealed relevant enriched biological processes and less expected ones. An enriched proportion of mitochondrial proteins at 15 min after biotin addition was observed. We propose that this result is due to ER-mitochondria membrane contacts sites and may not be relevant to the biosynthetic pathway of TfR.

Some Rabs can act together in the exocytosis process, such as Rab6 and Rab8 (*47*) or Rab3 and Rab27 (*48*). We detected >35% of TfR-eRUSH–containing vesicles harboring a Rab6-positive staining (Fig. 3D), but our data suggest, however, that Rab6 and Rab7 do not intervene at the same stage of the secretory pathway and/or in the same type of vesicular transport, as shown by the absence of overlap between the Rab6 and Rab7 staining (fig. S3B). Moreover, by TIRF microscopy (Fig. 5, D and E), we noticed two different processes of TfR transport using Rab6A or Rab7A, further indicating that these two Rabs likely correspond to two distinct secretory routes.

Combining results from the AP-MS/MS and siRNA screen, only one Rab was significantly standing out: Rab7. Rab7 is mostly known to mediate cargo trafficking between late endosomes and lysosomes (*35*), and it was unexpected to find it involved in the neosynthetic pathway. By electron microscopy, a group observed the presence of neosynthesized TfR inside endosome-like structures (*6*). Moreover, it was demonstrated that Rab7 was not involved in recycling of TfR at the PM, as depletion of Rab7A had no effect on TfR relocalization to the PM (*35*), and thus, it is unlikely that our observations would be the result of marginal PM-associated TfR endocytosis at early times after biotin addition.

A legitimate thought is to believe that the post-Golgi Rab7-decorated TfR-eRUSH vesicles correspond to a degradative pathway. However, extensive analyses of these vesicles show that they were mostly negative/dim to LysoTracker, they are neither proteolytically active (DQ-BSA marker) nor autophagosomes, and autophagy is not induced by the biotin treatment (Fig. 4). Moreover, the full membranes of the Western blot analysis show no degradative product, further demonstrating that TfR-eRUSH vesicles harboring Rab7 are not degradative, and actually, direct evidence supports PM targeting of these vesicles (Fig. 5D). However, the function of these vesicles as compared to the Rab6-positive vesicles remains to be determined.

A recent study by Chen *et al.* (*16*) indicated that neosynthesized TfR was sorted out with the Lamp1 protein in vesicles exiting the TGN, but they did not search for the presence of Rab7. Here, we show that a heterogeneous subset of TfR-containing vesicles exists, harboring Rab7 or Lamp1 or both. At this stage, it is difficult to ascertain the function of each subset, but one could envision that the triple-positive vesicles correspond to TfR and Lamp1 neosynthesized proteins cotransported into Rab7-positve vesicles. They also showed that these vesicles were devoid of the mannose-6P receptor (M6PR), which was used as a marker for the Golgi-to-endosome route (*49*). In our hands, we also found that M6PR was absent from the TfR-eRUSH vesicles harboring Rab7 (fig. S7). They concluded that the TfR^+ $Lamp1^+$ vesicles were bona fide secretory vesicles en route to the PM. In our study, a subset of vesicles containing TfR-eRUSH and Lamp1 was also decorated by Rab7 at time points corresponding to TGN exit. These vesicles may correlate with the ones described by Chen *et al.* (*16*), but their comprehensive composition and function in the secretory pathway remain to be fully determined.

We suggest that Rab7 could act as an intermediate compartment for neosynthesized TfR transport. Whether this Rab7 compartment corresponds to a bona fide late endosome remains unclear, as it does not exhibit the hallmarks of an acidic, pro-degradative vesicle. However, the neosynthesized TfR could traffic to specialized late endosomes destined to reach the PM, similar to exosome-containing multivesicular bodies. In this regard, Rab27A is a regulator of exosome secretion (*40*), and its silencing strongly prevents TfR arrival to the PM (Fig. 5A). It was previously shown that Rab7 and Rab27A may act one after another during the maturation process of melanosome (*50*). Future work should emphasize the link between the various Rabs along the biosynthetic secretory pathway.

Although the specific role of Rab7 on these secretory vesicles remains to be determined, one could hypothesize that Rab7 regulates the trafficking of cargos with specific posttranslational modifications. Alternatively, this pathway could transport cargos dedicated to specific PM domains. Recently, Rab7 has been mapped not only to late endosomes and lysosomes but also at the ER, TGN, and mitochondrial membranes, a localization maintained by the retromer complex (*51*), and thus, it is likely that Rab7 exerts pleiotropic roles.

MATERIALS AND METHODS

Cell culture

SUM159 cells were cultured in Dulbecco's modified Eagle's medium (DMEM)/F-12 GlutaMAX (GIBCO), supplemented with 5% fetal bovine serum (FBS; Dominique Dutscher), penicillin-streptomycin (500 μg/ml; GIBCO), hydrocortisone (1 μg/ml; Sigma-Aldrich), insulin (5 μg/ml; Sigma-Aldrich), and 10 mM Hepes (GIBCO) (complete medium). Cells were maintained at 37°C and 5% CO_2. For cytometry-based assay, Tf-A647 was diluted in DMEM/F-12 GlutaMAX (GIBCO), supplemented with 0.1% BSA, penicillin-streptomycin (500 μg/ml; GIBCO), hydrocortisone (1 μg/ml; Sigma-Aldrich), insulin (5 μg/ml; Sigma-Aldrich), and 10 mM Hepes (GIBCO; pH 7.0) (Tf medium).

Generation of the TfR-eRUSH CRISPR-Cas9–edited cell line

For gene editing of the SUM159 cells to fuse the GGSGGSGGS spacer, the SBP, and EGFP sequences to the C terminus of TfR, a CRISPR-Cas9 strategy was used as previously described (*22*, *52*).

Briefly, three genetic tools were cotransfected using the transfection reagent TransfeX (American Type Culture Collection): (i) a plasmid coding for CRISPR-associated protein 9 (Cas9), a template plasmid; (ii) a linear polymerase chain reaction (PCR) product used to transcribe the trans-activating crispr RNA (tracrRNA) and guide RNA targeting ATAGCTTCCATGAGAACAGC (corresponding to a region near the genomic TfR stop codon) under the control of the human U6 promoter; (iii) a donor DNA construct (serving as template during homologous recombination) corresponding to the spacer, SBP, and EGFP sequences flanked by ≈800 base pairs (bp) upstream and 800 bp downstream of the TfR stop codon. Single-cell sorting of EGFP-positive cells was performed, and homo/heterozygotic monoclonal cell lines expressing endogenous TfR-eRUSH were screened by PCR using the forward primer 5′-CTCACACGCTGCCAGCTTTA-3′ and the reverse primer 5′-TTCAGCAGAGACCAGCCCTT-3′.

A clone that was edited on both alleles was further transduced with a lentiviral vector coding the puromycin resistance gene and for the "hook" consisting of the streptavidin protein linked to the KDEL motif (*12*). Upon puromycin selection, the SUM159 TfR-eRUSH cells were expanded and stocks for the original tube were maintained in liquid nitrogen.

Plasmids

The Ruby3-Rab7A (Addgene plasmid #135651), Ruby3-Rab6A (Addgene plasmid #135653), and Ruby3-Rab10 cDNA constructs cloned into pBS vectors under the control of the weak promoter L30 were generated by the Montpellier Genomic Collection (MGC). The GFP-Rab7A (#61803) and GFP-Rab7A T22N (#28048) plasmids were obtained from Addgene. The siRNA-resistant GFP-Rab7A construct was generated using the forward primer 5′-AGTATTC-GATGTGACTGCCCCCAACAC-3′ and the reverse primer 5′-AG-TACACAGCAGTCTGCACCTCTGTAGAAG-3′. Site-directed mutagenesis was carried out using the Q5 Site-Directed Mutagenesis Kit (New England Biolabs) according to the manufacturer's instructions.

Antibodies and treatments

For immunofluorescence, primary antibodies used were mouse anti-GM130 (1:1000; BD Biosciences), sheep anti-TGN46 (1:1000; Bio-Rad), rabbit anti-calnexin (1:1000; Elabscience), mouse anti-Lamp1 (1:100; BD Biosciences), rabbit anti-Rab7 (1:250; Cell Signaling Technology), rabbit anti-Rab5 (1:1000; Cell Signaling Technology), rabbit anti-Rab6 (1:1000; Cell Signaling Technology), rabbit anti-Rab18 (1:200; Sigma-Aldrich), rabbit anti-TMED10 (1:500; Sigma-Aldrich), mouse anti-LC3 (1:1000; Sigma-Aldrich), and mouse anti-TfR (1:250; Miltenyi Biotec). Secondary antibodies used were Alexa Fluor 568 donkey anti-sheep (1:1000; Life Technologies), Alexa Fluor 568 donkey anti-rabbit (1:1000; Thermo Fisher Scientific), and Alexa Fluor 647 donkey anti-mouse (1:1000; Thermo Fisher Scientific). Antibodies used for immunoblotting were rabbit anti-TfR (1:1000; Aviva Systems Biology), mouse anti–β-actin (Abcam), mouse anti-GFP (1:1000; Sigma-Aldrich), rabbit anti-RILP (1:1000; Novus Biologicals), mouse anti-GAPDH (glyceraldehyde-3-phosphate dehydrogenase) (1:1000; Genetex), and rabbit anti-LC3 (1:1000; Sigma-Aldrich). Secondary antibodies used for immunoblotting were goat anti-mouse immunoglobulin G (IgG) horseradish peroxidase (HRP) antibody (1:10,000; Jackson ImmunoResearch) and goat anti-rabbit IgG HRP antibody (1:10,000; Jackson ImmunoResearch). Probes used for immunofluorescence were membrane-permeable MitoTracker Orange CM-H_2TMRos (Molecular Probes) used for 30 min at 100 nM to label mitochondria, LysoTracker Red (Life Technologies) for acidic compartments used for 30 min at 50 nM, DQ-Red BSA (Life Technologies) incubated for 6 hours at 10 μg/ml in complete medium, and DAPI (4′,6-diamidino-2-phenylindole) (1:1000; Sigma-Aldrich) used to stain the nucleus. For flow cytometry, Tf-A647 (Molecular Probes) was used at 10 μg/ml and mouse TfR antibody (10 μg/ml). For Western blotting, cells were treated for 4 hours with cycloheximide (50 μg/ml) and 100 nM Baf A1 before 30-min biotin incubation for TfR-eRUSH release. Cells were treated for 30 min with 40 nM apilimod before biotin treatment.

Cytometry-based RUSH assay

To detect PM-localized TfR, 50,000 SUM159 cells were plated in 24-well plates and incubated in complete medium containing avidin (0.2 μg/ml; Sigma-Aldrich) for 48 hours. To initiate TfR release, cells were incubated in a fresh complete medium containing 40 μM biotin (Sigma-Aldrich) for the indicated amount of time at 37°C and 5% CO_2. Then, cells were placed on ice, the medium was replaced with ice-cold phosphate-buffered saline (PBS), and cells were maintained at 4°C for 10 min. To measure the amount of TfR at the PM, cells were incubated for 30 min with Tf (10 μg/ml) coupled to an Alexa Fluor 647 (Tf-A647; Molecular probes) diluted in Tf medium. For acid wash treatment, cells were incubated in 0.1 M glycine (pH 3.0) for 2 min and then washed two times with cold PBS. In the absence of acid wash, unbound Tf-A647 was washed two times with cold PBS and cells were detached with 5 mM EDTA. Cells were collected and centrifuged at 500*g* for 5 min at 4°C. Cell fixation was carried out with 4% paraformaldehyde (PFA) for 15 min at room temperature, and after two washes, they were resuspended in a flow cytometry buffer [PBS (pH 7.0), 0.5% BSA, and 0.5 mM EDTA]. Samples were run on a CytoFLEX (Beckman Coulter) or NovoCyte (ACEA Biosciences) flow cytometer equipped with 488- and 640-nm lasers and four-filter set.

Small interfering RNA

A pool of four different siRNAs for each of the 12 selected Rab proteins and a nontargeting siRNA control were purchased as a custom-made siGENOME SMARTpool cherry-pick library (Dharmacon, Horizon Discovery; see details in table S3). Forty thousand SUM159 cells were seeded in 48-well plates, and on the next day, 3 pmol of siRNA was transfected using Lipofectamine 2000 (Thermo Fisher Scientific) according to the manufacturer's instructions. Cells were further incubated for 48 hours in complete medium in the presence of avidin (0.28 μg/ml). The day of the experiment, cells were incubated at different time points with 40 μM biotin. The cytometry-based assay for PM-localized TfR described above was used for sample analysis.

For single siRNA, siRNA control, siRNA Rab7, or siRNA RILP was purchased from Ambion, Thermo Fisher Scientific. Fifty thousand cells were seeded in 24-well plates, and the next day, 11 pmol of siRNA was transfected using Lipofectamine 3000 (Thermo Fisher Scientific).

Overexpression assays

In 24-well plates, 50,000 TfR-eRUSH cells were seeded in complete medium in the presence of avidin (2 μg/ml). The next day, 0.5 μg of DNA containing the different plasmids (GFP, GFP-Rab7, or GFP-Rab7 T22N) was transfected using jetPRIME (Polyplus) according to the manufacturer's instructions. Cells were incubated for 24 hours in complete medium containing avidin (2 μg/ml). The day of the experiment, the cytometry-based assay was carried out. Data were

analyzed on the GFP cell population of high intensity corresponding to the transfected cells.

MS-based quantitative proteomics

Sample preparation

The immunoprecipitated samples were resuspended in Laemmli buffer, and the antibody-conjugated magnetic beads were removed. Protein concentration was determined using the RC-DC protein assay (Bio-Rad) according to the manufacturer's instructions, and a standard curve was established using BSA. For each sample, 8 µg of protein lysate was concentrated on a stacking gel by electrophoresis. The gel bands were cut, washed with ammonium hydrogen carbonate and acetonitrile, reduced, and alkylated before trypsin digestion (Promega). The generated peptides were extracted with 60% acetonitrile in 0.1% formic acid followed by a second extraction with 100% acetonitrile. Acetonitrile was evaporated under vacuum, and the peptides were resuspended in 16 µl of H_2O and 0.1% formic acid before nanoLC-MS/MS analysis.

NanoLC-MS/MS analysis

NanoLC-MS/MS analyses were performed on a nanoACQUITY Ultra-Performance LC system (Waters, Milford, MA) coupled to a Q-Exactive Plus Orbitrap mass spectrometer (Thermo Fisher Scientific) equipped with a nanoelectrospray ion source. Samples were loaded into a Symmetry C18 precolumn (0.18 mm × 20 mm, 5 µm particle size; Waters) over 3 min in 1% solvent B (0.1% FA in acetonitrile) at a flow rate of 5 µl/min followed by reversed-phase separation (ACQUITY UPLC BEH130 C18, 200 mm × 75 µm inside diameter, 1.7 µm particle size; Waters) using a binary gradient ranging from 1 to 35% of solvent A (0.1% FA in H_2O) and solvent B at a flow rate of 450 nl/min. The mass spectrometer was operated in data-dependent acquisition mode by automatically switching between full MS and consecutive MS/MS acquisitions. Survey full-scan MS spectra (mass range of 300 to 1800) were acquired in the Orbitrap at a resolution of 70,000 at 200 *m/z* (mass/charge ratio) with an automatic gain control (AGC) fixed at 3×10^6 ions and a maximal injection time set to 50 ms. The 10 most intense peptide ions in each survey scan with a charge state of ≥2 were selected for MS/MS. MS/MS spectra were acquired at a resolution of 17,5 K at 200 *m/z*, with a fixed first mass at 100 *m/z*, AGC was set to 1×10^5, and the maximal injection time was set to 100 ms. Peptides were fragmented in the Higher-energy collisional dissociation (HCD) cell by higher-energy collisional dissociation with a normalized collision energy set to 27. Peaks selected for fragmentation were automatically included in a dynamic exclusion list for 60 s. All samples were injected using a randomized and blocked injection sequence (one biological replicate of each group plus pool in each block). To minimize carryover, a solvent blank injection was performed after each sample. A sample pool comprising equal amounts of all protein extracts was constituted and regularly injected four times during the course of the experiment, as an additional quality control (QC). Protein identification rates and coefficient of variation (CV) monitoring of this QC sample revealed very good stability of the system: 2207 of the 2271 (97%) identified proteins showed a CV value lower than 20% considering all four injections.

Data interpretation

Raw MS data processing was performed using MaxQuant software [v1.5.8.3 (*53*)]. Peak lists were searched against a composite database including all *Homo sapiens* protein sequences extracted from UniProtKB-SwissProt (version April 2019; taxonomy ID: 9606) using the MSDA (Mass Spectrometry Data Analysis) software suite (*54*). MaxQuant parameters were set as follows: MS tolerance set to 20 parts per million (ppm) for the first search and 5 ppm for the main search, MS/MS tolerance set to 40 ppm, maximum number of missed cleavages set to 1, carbamidomethyl (C) set as fixed modification, and acetyl (protein N terminus) and oxidation (M) set as variable modifications. FDRs were estimated on the basis of the number of hits after searching a reverse database and were set to 5% for both peptide spectrum matches (minimum length of seven amino acids) and proteins. Data normalization and protein quantification were performed using the label-free quantification option implemented in MaxQuant (*53*) using a "minimal ratio count" of two. The "match between runs" option was enabled using a 2-min time window after retention time alignment. All other MaxQuant parameters were set as default.

To be validated, proteins must be identified in all four replicates of one condition at least. The imputation of the missing values and differential data analysis were performed using the open-source ProStaR software (*55*). Two runs of imputation were applied: The "SLSA" mode was applied for the POVs (partially observed values) and the "del quantile" for the MEC (missing in the entire condition). Pairwise comparisons were performed using a Limma *t* test on protein intensities. *P* value calibration was performed using the pound calibration method, and the FDR threshold was set at 5%. The complete proteomics dataset is available via ProteomeXchange (*56*, *57*) with identifier PXD010576.

Gene ontology analysis

Gene set enrichment analysis (GSEA) was run on the protein lists found to be significantly enriched at least 1.5 times in T0-T15, T0-T30, and T15-T30 using the online molecular signature database MSigDB v6.2 (*24*). Significantly enriched gene ontology (GO) pathways related to relevant "biological process" were extracted with their FDR. Table S1 summarizes the relevant GO pathways associated to the T0-T15 time points. No significant enrichment was found at T0-T30 and T15-T30.

Fluorescence microscopy

Fifty thousand cells were plated on 24-well plates containing 12-mm cover glasses (Electron Microscopy Sciences) and incubated for 48 hours in complete medium containing avidin (1 µg /ml). For the different eRUSH assays, cells were incubated at 12, 15, and 30 min in complete medium containing 40 µM biotin. Cells were fixed with 4% PFA for 20 min at room temperature and permeabilized for 15 min with PBS containing 0.1% Triton X-100 (Sigma-Aldrich) and 0.5% BSA (Euromedex). Cells were subsequently incubated for 1 hour at room temperature with different primary antibodies (see the "Antibodies and treatments" section) and then 1 hour with secondary antibodies and DAPI staining. Cells were mounted with Mowiol 4-88 (Sigma-Aldrich). For LC3 staining, cells were fixed with formalin (Sigma-Aldrich) for 15 min at room temperature and then with cold methanol for 5 min at −20°C, before antibody staining in PBS containing 0.1% saponin and 1% FBS.

Images were taken with an Axio Observer Z1 inverted microscope (Zeiss) mounted with a CSU-X1 spinning disk head (Yokogawa), a back-illuminated Electron-multiplying charge-coupled device (EMCCD) camera (Evolve, Photometrics), and 63× [1.45 numerical aperture (NA)] or 100× (1.45 NA) oil objectives (Zeiss). Images were processed with Fiji software and presented as single z-stack for visualization of the co-distribution.

Live imaging

About 250,000 cells seeded on 35-mm #1.5 glass-bottom dishes (Ibidi) or on 25-mm cover glasses (Electron Microscopy Sciences) were

transfected using jetPRIME (Polyplus Transfection) according to the manufacturer's instructions. The dish was placed on the microscope stage and maintained in a dark atmosphere–controlled chamber at 37°C and 5% CO_2. Live-cell imaging was performed using an Axio Observer Z1 inverted microscope (Zeiss) mounted with a CSU-X1 spinning disk head (Yokogawa), a back-illuminated EMCCD camera (Evolve, Photometrics), and a 100× (1.45 NA) oil objective (Zeiss) controlled by VisiView v.3.3.0 software (Visitron Systems). For TIRF microscopy, live imaging was performed with a TIRF PALM STORM microscope from Nikon using a back-illuminated EMCCD camera (Evolve 512, Photometrics) and a 100× APO (1.49 NA) oil objective controlled by MetaMorph and an iLas^2 FRAP/TIRF module (BioVision Technologies). The TIRF angle was chosen to obtain a calculated evanescent field depth of <100 nm. Acquisition was performed from 5 to 25 min after biotin addition. Images were processed with FiJi software and presented as single z-stack for visualization of the co-distribution.

Preparation of protein extracts

Cells (250,000 per well) were seeded in a six-well plate in complete medium containing avidin (1 μg/ml) for 48 hours. After incubation with biotin for 0 or 30 min, cells were washed three times with ice-cold PBS and lysed with ice-cold radioimmunoprecipitation assay buffer [150 mM sodium chloride, 1% NP-40, 0.5% sodium deoxycholate, 0.1% SDS, 50 mM tris (pH 8.0), and protease inhibitor (Promega)]. Cells were placed on ice for 10 min and spun at 10,000*g* for 20 min at 4°C. The supernatant was collected and subjected to the Pierce BCA Assay Kit (Thermo Fisher Scientific).

Western blot analysis

A total of 20 or 40 μg of protein lysates were run on Bolt 4 to 12% Bis-Tris plus gels (Thermo Fisher Scientific), and proteins were transferred to nitrocellulose membranes. Nitrocellulose membranes were blocked with 5% (w/v) milk in PBS-T [PBS (pH 7.4) and 0.05% Tween 20] for 15 min. Primary antibodies (refer to the "Antibodies and treatments" section) were incubated for 1 hour at room temperature or overnight at 4°C in PBS-T containing 5% milk. Secondary antibodies were incubated for 1 hour at room temperature. After washing with PBS-T, nitrocellulose membranes were incubated with Clarity Max Western ECL Substrate (Bio-Rad). The specific proteins were visualized with the ChemiDoc imaging system (Bio-Rad).

Software analysis

Image processing was performed using either the Fiji upgrade of ImageJ (*58*) or Imaris software v9.2 (Bitplane, Oxford Instruments). Quantifications for colocalization measurements were performed using Imaris software v9.2 (Bitplane, Oxford Instruments). Statistical analyses were performed with Microsoft Excel 2016 and Prism v7.04 (GraphPad). Flow cytometry analysis was done using FlowJo software v10.4.2 (FlowJo LLC). Raw MS data were first analyzed using MaxQuant v1.6.0.16. Differential proteomics data analysis was performed using DAPAR v1.10.3 and ProStaR v1.10.4.

SUPPLEMENTARY MATERIALS

Supplementary material for this article is available at http://advances.sciencemag.org/cgi/content/full/7/2/eaba7803/DC1

View/request a protocol for this paper from *Bio-protocol*.

REFERENCES AND NOTES

1. R. B. Kelly, Pathways of protein secretion in eukaryotes. *Science* **230**, 25–32 (1985).
2. L. Zhao, P. Liu, G. Boncompain, F. Loos, S. Lachkar, L. Bezu, G. Chen, H. Zhou, F. Perez, O. Kepp, G. Kroemer, Identification of pharmacological inhibitors of conventional protein secretion. *Sci. Rep.* **8**, 14966 (2018).
3. D. Jensen, R. Schekman, COPII-mediated vesicle formation at a glance. *J. Cell Sci.* **124**, 1–4 (2011).
4. A. Luini, A brief history of the cisternal progression–maturation model. *Cell Logist.* **1**, 6–11 (2011).
5. M. H. Dunlop, A. M. Ernst, L. K. Schroeder, D. K. Toomre, G. Lavieu, J. E. Rothman, Land-locked mammalian Golgi reveals cargo transport between stable cisternae. *Nat. Commun.* **8**, 432 (2017).
6. C. E. Futter, C. N. Connolly, D. F. Cutler, C. R. Hopkins, Newly synthesized transferrin receptors can be detected in the endosome before they appear on the cell surface. *J. Biol. Chem.* **270**, 10999–11003 (1995).
7. A. L. Ang, T. Taguchi, S. Francis, H. Fölsch, L. J. Murrells, M. Pypaert, G. Warren, I. Mellman, Recycling endosomes can serve as intermediates during transport from the Golgi to the plasma membrane of MDCK cells. *J. Cell Biol.* **167**, 531–543 (2004).
8. J. G. Lock, J. L. Stow, Rab11 in recycling endosomes regulates the sorting and basolateral transport of E-cadherin. *Mol. Biol. Cell* **16**, 1744–1755 (2005).
9. K. O. Cresawn, B. A. Potter, A. Oztan, C. J. Guerriero, G. Ihrke, J. R. Goldenring, G. Apodaca, O. A. Weisz, Differential involvement of endocytic compartments in the biosynthetic traffic of apical proteins. *EMBO J.* **26**, 3737–3748 (2007).
10. W. E. Balch, J. M. McCaffery, H. Plutner, M. G. Farquhar, Vesicular stomatitis virus glycoprotein is sorted and concentrated during export from the endoplasmic reticulum. *Cell* **76**, 841–852 (1994).
11. J. F. Presley, N. B. Cole, T. A. Schroer, K. Hirschberg, K. J. Zaal, J. Lippincott-Schwartz, ER-to-Golgi transport visualized in living cells. *Nature* **389**, 81–85 (1997).
12. G. Boncompain, S. Divoux, N. Gareil, H. de Forges, A. Lescure, L. Latreche, V. Mercanti, F. Jollivet, G. Raposo, F. Perez, Synchronization of secretory protein traffic in populations of cells. *Nat. Methods* **9**, 493–498 (2012).
13. F. Loos, W. Xie, V. Sica, J. M. Bravo-San Pedro, S. Souquère, G. Pierron, S. Lachkar, A. Sauvat, A. Petrazzuolo, A. J. Jimenez, F. Perez, M. C. Maiuri, O. Kepp, G. Kroemer, Artificial tethering of LC3 or p62 to organelles is not sufficient to trigger autophagy. *Cell Death Dis.* **10**, 771 (2019).
14. L. Fourriere, A. Kasri, N. Gareil, S. Bardin, H. Bousquet, D. Pereira, F. Perez, B. Goud, G. Boncompain, S. Miserey-Lenkei, RAB6 and microtubules restrict protein secretion to focal adhesions. *J. Cell Biol.* **218**, 2215–2231 (2019).
15. L. C. Gomes-da-Silva, L. Zhao, L. Bezu, H. Zhou, A. Sauvat, P. Liu, S. Durand, M. Leduc, S. Souquere, F. Loos, L. Mondragón, B. Sveinbjørnsson, Ø. Rekdal, G. Boncompain, F. Perez, L. G. Arnaut, O. Kepp, G. Kroemer, Photodynamic therapy with redaporfin targets the endoplasmic reticulum and Golgi apparatus. *EMBO J.* **37**, e98354 (2018).
16. Y. Chen, D. C. Gershlick, S. Y. Park, J. S. Bonifacino, Segregation in the Golgi complex precedes export of endolysosomal proteins in distinct transport carriers. *J. Cell Biol.* **216**, 4141–4151 (2017).
17. B. D. Grant, J. G. Donaldson, Pathways and mechanisms of endocytic recycling. *Nat. Rev. Mol. Cell Biol.* **10**, 597–608 (2009).
18. C. J. Greene, K. Attwood, N. J. Sharma, K. W. Gross, G. J. Smith, B. Xu, E. C. Kauffman, Transferrin receptor 1 upregulation in primary tumor and downregulation in benign kidney is associated with progression and mortality in renal cell carcinoma patients. *Oncotarget* **8**, 107052–107075 (2017).
19. C. Raggi, E. Gammella, M. Correnti, P. Buratti, E. Forti, J. B. Andersen, G. Alpini, S. Glaser, D. Alvaro, P. Invernizzi, G. Cairo, S. Recalcati, Dysregulation of iron metabolism in cholangiocarcinoma stem-like cells. *Sci. Rep.* **7**, 17667 (2017).
20. R. Taetle, J. M. Honeysett, I. Trowbridge, Effects of anti-transferrin receptor antibodies on growth of normal and malignant myeloid cells. *Int. J. Cancer* **32**, 343–349 (1983).
21. T. R. Daniels, E. Bernabeu, J. A. Rodríguez, S. Patel, M. Kozman, D. A. Chiappetta, E. Holler, J. Y. Ljubimova, G. Helguera, M. L. Penichet, The transferrin receptor and the targeted delivery of therapeutic agents against cancer. *Biochim. Biophys. Acta* **1820**, 291–317 (2012).
22. Y.-Y. Chou, C. Cuevas, M. Carocci, S. H. Stubbs, M. Ma, D. K. Cureton, L. Chao, F. Evesson, K. He, P. L. Yang, S. P. Whelan, S. R. Ross, T. Kirchhausen, R. Gaudin, Identification and characterization of a novel broad-spectrum virus entry inhibitor. *J. Virol.* **90**, 4494–4510 (2016).
23. D. Szklarczyk, A. Franceschini, S. Wyder, K. Forslund, D. Heller, J. Huerta-Cepas, M. Simonovic, A. Roth, A. Santos, K. P. Tsafou, M. Kuhn, P. Bork, L. J. Jensen, C. von Mering, STRING v10: Protein–protein interaction networks, integrated over the tree of life. *Nucleic Acids Res.* **43**, D447–D452 (2015).
24. A. Subramanian, P. Tamayo, V. K. Mootha, S. Mukherjee, B. L. Ebert, M. A. Gillette, A. Paulovich, S. L. Pomeroy, T. R. Golub, E. S. Lander, J. P. Mesirov, Gene set enrichment analysis: A knowledge-based approach for interpreting genome-wide expression profiles. *Proc. Natl. Acad. Sci. U.S.A.* **102**, 15545–15550 (2005).

25. C. Bonnon, M. W. Wendeler, J.-P. Paccaud, H.-P. Hauri, Selective export of human GPI-anchored proteins from the endoplasmic reticulum. *J. Cell Sci.* **123**, 1705–1715 (2010).
26. M. E. Coulter, C. M. Dorobantu, G. A. Lodewijk, F. Delalande, S. Cianferani, V. S. Ganesh, R. S. Smith, E. T. Lim, C. S. Xu, S. Pang, E. T. Wong, H. G. W. Lidov, M. L. Calicchio, E. Yang, D. M. Gonzalez, T. M. Schlaeger, G. H. Mochida, H. Hess, W.-C. A. Lee, M. K. Lehtinen, T. Kirchhausen, D. Haussler, F. M. J. Jacobs, R. Gaudin, C. A. Walsh, The ESCRT-III protein CHMP1A mediates secretion of sonic hedgehog on a distinctive subtype of extracellular vesicles. *Cell Rep.* **24**, 973–986.e8 (2018).
27. R. Rizzuto, P. Pinton, W. Carrington, F. S. Fay, K. E. Fogarty, L. M. Lifshitz, R. A. Tuft, T. Pozzan, Close contacts with the endoplasmic reticulum as determinants of mitochondrial Ca^{2+} responses. *Science* **280**, 1763–1766 (1998).
28. A. Das, S. Nag, A. B. Mason, M. M. Barroso, Endosome–mitochondria interactions are modulated by iron release from transferrin. *J. Cell Biol.* **214**, 831–845 (2016).
29. H. Plutner, A. D. Cox, S. Pind, R. Khosravi-Far, J. R. Bourne, R. Schwaninger, C. J. Der, W. E. Balch, Rab1b regulates vesicular transport between the endoplasmic reticulum and successive Golgi compartments. *J. Cell Biol.* **115**, 31–43 (1991).
30. S. Y. Dejgaard, A. Murshid, A. Erman, Ö. Kizilay, D. Verbich, R. Lodge, K. Dejgaard, T. B. N. Ly-Hartig, R. Pepperkok, J. C. Simpson, J. F. Presley, Rab18 and Rab43 have key roles in ER-Golgi trafficking. *J. Cell Sci.* **121**, 2768–2781 (2008).
31. A. J. Isabella, S. Horne-Badovinac, Rab10-mediated secretion synergizes with tissue movement to build a polarized basement membrane architecture for organ morphogenesis. *Dev. Cell* **38**, 47–60 (2016).
32. K. N. Kitt, D. Hernández-Deviez, S. D. Ballantyne, E. T. Spiliotis, J. E. Casanova, J. M. Wilson, Rab14 regulates apical targeting in polarized epithelial cells. *Traffic* **9**, 1218–1231 (2008).
33. S. Seto, K. Tsujimura, Y. Koide, Rab GTPases regulating phagosome maturation are differentially recruited to mycobacterial phagosomes. *Traffic* **12**, 407–420 (2011).
34. T. Matsui, T. Itoh, M. Fukuda, Small GTPase Rab12 regulates constitutive degradation of transferrin receptor. *Traffic* **12**, 1432–1443 (2011).
35. P. A. Vanlandingham, B. P. Ceresa, Rab7 regulates late endocytic trafficking downstream of multivesicular body biogenesis and cargo sequestration. *J. Biol. Chem.* **284**, 12110–12124 (2009).
36. X. Cai, Y. Xu, A. K. Cheung, R. C. Tomlinson, A. Alcázar-Román, L. Murphy, A. Billich, B. Zhang, Y. Feng, M. Klumpp, J.-M. Rondeau, A. N. Fazal, C. J. Wilson, V. Myer, G. Joberty, T. Bouwmeester, M. A. Labow, P. M. Finan, J. A. Porter, H. L. Ploegh, D. Baird, P. De Camilli, J. A. Tallarico, Q. Huang, PIKfyve, a class III PI kinase, is the target of the small molecular IL-12/IL-23 inhibitor apilimod and a player in toll-like receptor signaling. *Chem. Biol.* **20**, 912–921 (2013).
37. C. Bucci, P. Thomsen, P. Nicoziani, J. McCarthy, B. van Deurs, Rab7: A key to lysosome biogenesis. *Mol. Biol. Cell* **11**, 467–480 (2000).
38. D. J. Klionsky, K. Abdelmohsen, A. Abe, M. J. Abedin, H. Abeliovich, A. A. Arozena, H. Adachi, C. M. Adams, P. D. Adams, K. Adeli, P. J. Adhihetty, S. G. Adler, G. Agam, R. Agarwal, M. K. Aghi, M. Agnello, P. Agostinis, P. V. Aguilar, J. Aguirre-Ghiso, E. M. Airoldi, S. Ait-Si-Ali, T. Akematsu, E. T. Akporiaye, M. Al-Rubeai, G. M. Albaiceta, C. Albanese, D. Albani, M. L. Albert, J. Aldudo, H. Algül, M. Alirezaei, I. Alloza, A. Almasan, M. Almonte-Beceril, E. S. Alnemri, C. Alonso, N. Altan-Bonnet, D. C. Altieri, S. Alvarez, L. Alvarez-Erviti, S. Alves, G. Amadoro, A. Amano, C. Amantini, S. Ambrosio, I. Amelio, A. O. Amer, M. Amessou, A. Amon, Z. An, F. A. Anania, S. U. Andersen, U. P. Andley, C. K. Andreadi, N. Andrieu-Abadie, A. Anel, D. K. Ann, S. Anoopkumar-Dukie, M. Antonioli, H. Aoki, N. Apostolova, S. Aquila, K. Aquilano, K. Araki, E. Arama, A. Aranda, J. Araya, A. Arcaro, E. Arias, H. Arimoto, A. R. Ariosa, J. L. Armstrong, T. Arnould, I. Arsov, K. Asanuma, V. Askanas, E. Asselin, R. Atarashi, S. S. Atherton, J. D. Atkin, L. D. Attardi, P. Auberger, G. Auburger, L. Aurelian, R. Autelli, L. Avagliano, M. L. Avantaggiati, L. Avrahami, S. Awale, N. Azad, T. Bachetti, J. M. Backer, D.-H. Bae, J.-S. Bae, O.-N. Bae, S. H. Bae, E. H. Baehrecke, S.-H. Baek, S. Baghdiguian, A. Bagniewska-Zadworna, H. Bai, J. Bai, X.-Y. Bai, Y. Bailly, K. N. Balaji, W. Balduini, A. Ballabio, R. Balzan, R. Banerjee, G. Bánhegyi, H. Bao, B. Barbeau, M. D. Barrachina, E. Barreiro, B. Bartel, A. Bartolomé, D. C. Bassham, M. T. Bassi, R. C. Bast Jr, A. Basu, M. T. Batista, H. Batoko, M. Battino, K. Bauckman, B. L. Baumgarner, K. U. Bayer, R. Beale, J.-F. Beaulieu, G. R. Beck Jr, C. Becker, J. D. Beckham, P.-A. Bédard, P. J. Bednarski, T. J. Begley, C. Behl, C. Behrends, G. M. Behrens, K. E. Behrns, E. Bejarano, A. Belaid, F. Belleudi, G. Bénard, G. Berchem, D. Bergamaschi, M. Bergami, B. Berkhout, L. Berliocchi, A. Bernard, M. Bernard, F. Bernassola, A. Bertolotti, A. S. Bess, S. Besteiro, S. Bettuzzi, S. Bhalla, S. Bhattacharyya, S. K. Bhutia, C. Biagosch, M. W. Bianchi, M. Biard-Piechaczyk, V. Billes, C. Bincoletto, B. Bingol, S. W. Bird, M. Bitoun, I. Bjedov, C. Blackstone, L. Blanc, G. A. Blanco, H. K. Blomhoff, E. Boada-Romero, S. Böckler, M. Boes, K. Boesze-Battaglia, L. H. Boise, A. Bolino, A. Boman, P. Bonaldo, M. Bordi, J. Bosch, L. M. Botana, J. Botti, G. Bou, M. Bouché, M. Bouchecareilh, M.-J. Boucher, M. E. Boulton, S. G. Bouret, P. Boya, M. Boyer-Guittaut, P. V. Bozhkov, N. Brady, V. M. Braga, C. Brancolini, G. H. Braus, J. M. Bravo-San Pedro, L. A. Brennan, E. H. Bresnick, P. Brest, D. Bridges, M.-A. Bringer, M. Brini, G. C. Brito, B. Brodin, P. S. Brookes, E. J. Brown, K. Brown, H. E. Broxmeyer, A. Bruhat, P. C. Brum, J. H. Brumell, N. Brunetti-Pierri, R. J. Bryson-Richardson, S. Buch, A. M. Buchan, H. Budak, D. V. Bulavin, S. J. Bultman, G. Bultynck, V. Bumbasirevic, Y. Burelle, R. E. Burke, M. Burmeister, P. Bütikofer, L. Caberlotto, K. Cadwell, M. Cahova, D. Cai, J. Cai, Q. Cai, S. Calatayud, N. Camougrand, M. Campanella, G. R. Campbell, M. Campbell, S. Campello, R. Candau, I. Caniggia, L. Cantoni, L. Cao, A. B. Caplan, M. Caraglia, C. Cardinali, S. M. Cardoso, J. S. Carew, L. A. Carleton, C. R. Carlin, S. Carloni, S. R. Carlsson, D. Carmona-Gutierrez, L. A. Carneiro, O. Carnevali, S. Carra, A. Carrier, B. Carroll, C. Casas, J. Casas, G. Cassinelli, P. Castets, S. Castro-Obregon, G. Cavallini, I. Ceccherini, F. Cecconi, A. I. Cederbaum, V. Ceña, S. Cenci, C. Cerella, D. Cervia, S. Cetrullo, H. Chaachouay, H.-J. Chae, A. S. Chagin, C.-Y. Chai, G. Chakrabarti, G. Chamilos, E. Y. Chan, M. T. Chan, D. Chandra, P. Chandra, C.-P. Chang, R. C.-C. Chang, T. Y. Chang, J. C. Chatham, S. Chatterjee, S. Chauhan, Y. Che, M. E. Cheetham, R. Cheluvappa, C.-J. Chen, G. Chen, G.-C. Chen, G. Chen, H. Chen, J. W. Chen, J.-K. Chen, M. Chen, M. Chen, P. Chen, Q. Chen, Q. Chen, S.-D. Chen, S. Chen, S. S.-L. Chen, W. Chen, W.-J. Chen, W. Q. Chen, W. Chen, X. Chen, Y.-H. Chen, Y.-G. Chen, Y. Chen, Y. Chen, Y.-J. Chen, Y.-Q. Chen, Y. Chen, Z. Chen, Z. Chen, A. Cheng, C. H. Cheng, H. Cheng, H. Cheong, S. Cherry, J. Chesney, C. H. A. Cheung, E. Chevet, H. C. Chi, S.-G. Chi, F. Chiacchiera, H.-L. Chiang, R. Chiarelli, M. Chiariello, M. Chieppa, L.-S. Chin, M. Chiong, G. N. Chiu, D.-H. Cho, S.-G. Cho, W. C. Cho, Y.-Y. Cho, Y.-S. Cho, A. M. Choi, E.-J. Choi, E.-K. Choi, J. Choi, M. E. Choi, S.-I. Choi, T.-F. Chou, S. Chouaib, D. Choubey, V. Choubey, K.-C. Chow, K. Chowdhury, C. T. Chu, T.-H. Chuang, T. Chun, H. Chung, T. Chung, Y.-L. Chung, Y.-J. Chwae, V. Cianfanelli, R. Ciarcia, I. A. Ciechomska, M. R. Ciriolo, M. Cirone, S. Claerhout, M. J. Clague, J. Clària, P. G. Clarke, R. Clarke, E. Clementi, C. Cleyrat, M. Cnop, E. M. Coccia, T. Cocco, P. Codogno, J. Coers, E. E. Cohen, D. Colecchia, L. Coletto, N. S. Coll, E. Colucci-Guyon, S. Comincini, M. Condello, K. L. Cook, G. H. Coombs, C. D. Cooper, J. M. Cooper, I. Coppens, M. T. Corasaniti, M. Corazzari, R. Corbalan, E. Corcelle-Termeau, M. D. Cordero, C. Corral-Ramos, O. Corti, A. Cossarizza, P. Costelli, S. Costes, S. L. Cotman, A. Coto-Montes, S. Cottet, E. Couve, L. R. Covey, L. A. Cowart, J. S. Cox, F. P. Coxon, C. B. Coyne, M. S. Cragg, R. J. Craven, T. Crepaldi, J. L. Crespo, A. Criollo, V. Crippa, M. T. Cruz, A. M. Cuervo, J. M. Cuezva, T. Cui, P. R. Cutillas, M. J. Czaja, M. F. Czyzyk-Krzeska, R. K. Dagda, U. Dahmen, C. Dai, W. Dai, Y. Dai, K. N. Dalby, L. D. Valle, G. Dalmasso, M. D'Amelio, M. Damme, A. Darfeuille-Michaud, C. Dargemont, V. M. Darley-Usmar, S. Dasarathy, B. Dasgupta, S. Dash, C. R. Dass, H. M. Davey, L. M. Davids, D. Dávila, R. J. Davis, T. M. Dawson, V. L. Dawson, P. Daza, J. de Belleroche, P. de Figueiredo, R. C. B. Q. de Figueiredo, J. de la Fuente, L. De Martino, A. De Matteis, G. R. De Meyer, A. De Milito, M. De Santi, W. de Souza, V. De Tata, D. De Zio, J. Debnath, R. Dechant, J.-P. Decuypere, S. Deegan, B. Dehay, B. D. Bello, D. P. Del Re, R. Delage-Mourroux, L. M. Delbridge, L. Deldicque, E. Delorme-Axford, Y. Deng, J. Dengjel, M. Denizot, P. Dent, C. J. Der, V. Deretic, B. Derrien, E. Deutsch, T. P. Devarenne, R. J. Devenish, S. D. Bartolomeo, N. D. Daniele, F. D. Domenico, A. D. Nardo, S. D. Paola, A. D. Pietro, L. D. Renzo, A. D. Antonio, G. Díaz-Araya, I. Díaz-Laviada, M. T. Diaz-Meco, J. Diaz-Nido, C. A. Dickey, R. C. Dickson, M. Diederich, P. Digard, I. Dikic, S. P. Dinesh-Kumar, C. Ding, W.-X. Ding, Z. Ding, L. Dini, J. H. Distler, A. Diwan, M. Djavaheri-Mergny, K. Dmytruk, R. C. Dobson, V. Doetsch, K. Dokladny, S. Dokudovskaya, M. Donadelli, X. C. Dong, X. Dong, Z. Dong, T. M. Donohue Jr, K. S. Doran, G. D'Orazi, G. W. Dorn II, V. Dosenko, S. Dridi, L. Drucker, J. Du, L.-L. Du, L. Du, A. du Toit, P. Dua, L. Duan, P. Duann, V. K. Dubey, M. R. Duchen, M. A. Duchosal, H. Duez, I. Dugail, V. I. Dumit, M. C. Duncan, E. A. Dunlop, W. A. Dunn Jr, N. Dupont, L. Dupuis, R. V. Durán, T. M. Durcan, S. Duvezin-Caubet, U. Duvvuri, V. Eapen, D. Ebrahimi-Fakhari, A. Echard, L. Eckhart, C. L. Edelstein, A. L. Edinger, L. Eichinger, T. Eisenberg, A. Eisenberg-Lerner, N. T. Eissa, W. S. El-Deiry, V. El-Khoury, Z. Elazar, H. Eldar-Finkelman, C. J. Elliott, E. Emanuele, U. Emmenegger, N. Engedal, A.-M. Engelbrecht, S. Engelender, J. M. Enserink, R. Erdmann, J. Erenpreisa, R. Eri, J. L. Eriksen, A. Erman, R. Escalante, E.-L. Eskelinen, L. Espert, L. Esteban-Martínez, T. J. Evans, M. Fabri, G. Fabrias, C. Fabrizi, A. Facchiano, N. J. Færgeman, A. Faggioni, W. D. Fairlie, C. Fan, D. Fan, J. Fan, S. Fang, M. Fanto, A. Fanzani, T. Farkas, M. Faure, F. B. Favier, H. Fearnhead, M. Federici, E. Fei, T. C. Felizardo, H. Feng, Y. Feng, Y. Feng, T. A. Ferguson, Á. F. Fernández, M. G. Fernandez-Barrena, J. C. Fernandez-Checa, A. Fernández-López, M. E. Fernandez-Zapico, O. Feron, E. Ferraro, C. V. Ferreira-Halder, L. Fesus, R. Feuer, F. C. Fiesel, E. C. Filippi-Chiela, G. Filomeni, G. M. Fimia, J. H. Fingert, S. Finkbeiner, T. Finkel, F. Fiorito, P. B. Fisher, M. Flajolet, F. Flamigni, O. Florey, S. Florio, R. A. Floto, M. Folini, C. Follo, E. A. Fon, F. Fornai, F. Fortunato, A. Fraldi, R. Franco, A. Francois, A. François, L. B. Frankel, I. D. Fraser, N. Frey, D. G. Freyssenet, C. Frezza, S. L. Friedman, D. E. Frigo, D. Fu, J. M. Fuentes, J. Fueyo, Y. Fujitani, Y. Fujiwara, M. Fujiya, M. Fukuda, S. Fulda, C. Fusco, B. Gabryel, M. Gaestel, P. Gailly, M. Gajewska, S. Galadari, G. Galili, I. Galindo, M. F. Galindo, G. Galliciotti, L. Galluzzi, L. Galluzzi, V. Galy, N. Gammoh, S. Gandy, A. K. Ganesan, S. Ganesan, I. G. Ganley, M. Gannagé, F.-B. Gao, F. Gao, J.-X. Gao, L. G. Nannig, E. G. Véscovi, M. Garcia-Macía, C. Garcia-Ruiz, A. D. Garg, P. K. Garg, R. Gargini, N. C. Gassen, D. Gatica, E. Gatti, J. Gavard, E. Gavathiotis, L. Ge, P. Ge, S. Ge, P.-W. Gean, V. Gelmetti, A. A. Genazzani, J. Geng, P. Genschik, L. Gerner, J. E. Gestwicki, D. A. Gewirtz, S. Ghavami, E. Ghigo, D. Ghosh, A. M. Giammarioli, F. Giampieri, C. Giampietri, A. Giatromanolaki, D. J. Gibbings, L. Gibellini, S. B. Gibson, V. Ginet, A. Giordano, F. Giorgini, E. Giovannetti, S. E. Girardin, S. Gispert, S. Giuliano, C. L. Gladson, A. Glavic, M. Gleave, N. Godefroy, R. M. Gogal Jr, K. Gokulan, G. H. Goldman, D. Goletti, M. S. Goligorsky, A. V. Gomes, L. C. Gomes, H. Gomez, C. Gomez-Manzano, R. Gómez-Sánchez,

D. A. Gonçalves, E. Goncu, Q. Gong, C. Gongora, C. B. Gonzalez, P. Gonzalez-Alegre, P. Gonzalez-Cabo, R. A. González-Polo, I. S. Goping, C. Gorbea, N. V. Gorbunov, D. R. Goring, A. M. Gorman, S. M. Gorski, S. Goruppi, S. Goto-Yamada, C. Gotor, R. A. Gottlieb, I. Gozes, D. Gozuacik, Y. Graba, M. Graef, G. E. Granato, G. D. Grant, S. Grant, G. L. Gravina, D. R. Green, A. Greenhough, M. T. Greenwood, B. Grimaldi, F. Gros, C. Grose, J.-F. Groulx, F. Gruber, P. Grumati, T. Grune, J.-L. Guan, K.-L. Guan, B. Guerra, C. Guillen, K. Gulshan, J. Gunst, C. Guo, L. Guo, M. Guo, W. Guo, X.-G. Guo, A. A. Gust, Å. B. Gustafsson, E. Gutierrez, M. G. Gutierrez, H.-S. Gwak, A. Haas, J. E. Haber, S. Hadano, M. Hagedorn, D. R. Hahn, A. J. Halayko, A. Hamacher-Brady, K. Hamada, A. Hamai, A. Hamann, M. Hamasaki, I. Hamer, Q. Hamid, E. M. Hammond, F. Han, W. Han, J. T. Handa, J. A. Hanover, M. Hansen, M. Harada, L. Harhaji-Trajkovic, J. W. Harper, A. H. Harrath, A. L. Harris, J. Harris, U. Hasler, P. Hasselblatt, K. Hasui, R. G. Hawley, T. S. Hawley, C. He, C. Y. He, F. He, G. He, R.-R. He, X.-H. He, Y.-W. He, Y.-Y. He, J. K. Heath, M.-J. Hébert, R. A. Heinzen, G. V. Helgason, M. Hensel, E. P. Henske, C. Her, P. K. Herman, A. Hernández, C. Hernandez, S. Hernández-Tiedra, C. Hetz, P. R. Hiesinger, K. Higaki, S. Hilfiker, B. G. Hill, J. A. Hill, W. D. Hill, K. Hino, D. Hofius, P. Hofman, G. U. Höglinger, J. Höhfeld, M. K. Holz, Y. Hong, D. A. Hood, J. J. Hoozemans, T. Hoppe, C. Hsu, C.-Y. Hsu, L.-C. Hsu, D. Hu, G. Hu, H.-M. Hu, H. Hu, M. C. Hu, Y.-C. Hu, Z.-W. Hu, F. Hua, Y. Hua, C. Huang, H.-L. Huang, K.-H. Huang, K.-Y. Huang, S. Huang, S. Huang, W.-P. Huang, Y.-R. Huang, Y. Huang, Y. Huang, T. B. Huber, P. Huebbe, W.-K. Huh, J. J. Hulmi, G. M. Hur, J. H. Hurley, Z. Husak, S. N. Hussain, S. Hussain, J. J. Hwang, S. Hwang, T. I. Hwang, A. Ichihara, Y. Imai, C. Imbriano, M. Inomata, T. Into, V. Iovane, J. L. Iovanna, R. V. Iozzo, N. Y. Ip, J. E. Irazoqui, P. Iribarren, Y. Isaka, A. J. Isakovic, H. Ischiropoulos, J. S. Isenberg, M. Ishaq, H. Ishida, I. Ishii, J. E. Ishmael, C. Isidoro, K.-I. Isobe, E. Isono, S. Issazadeh-Navikas, K. Itahana, E. Itakura, A. I. Ivanov, A. K. V. Iyer, J. M. Izquierdo, Y. Izumi, V. Izzo, M. Jäättelä, N. Jaber, D. J. Jackson, W. T. Jackson, T. G. Jacob, T. S. Jacques, C. Jagannath, A. Jain, N. R. Jana, B. K. Jang, A. Jani, B. Janji, P. R. Jannig, P. J. Jansson, S. Jean, M. Jendrach, J.-H. Jeon, N. Jessen, E.-B. Jeung, K. Jia, L. Jia, H. Jiang, H. Jiang, L. Jiang, T. Jiang, X. Jiang, X. Jiang, X. Jiang, Y. Jiang, Y. Jiang, A. Jiménez, C. Jin, H. Jin, L. Jin, M. Jin, S. Jin, U. K. Jinwal, E.-K. Jo, T. Johansen, D. E. Johnson, G. V. Johnson, J. D. Johnson, E. Jonasch, C. Jones, L. A. Joosten, J. Jordan, A.-M. Joseph, B. Joseph, A. M. Joubert, D. Ju, J. Ju, H.-F. Juan, K. Juenemann, G. Juhász, H. S. Jung, J. U. Jung, Y.-K. Jung, H. Jungbluth, M. J. Justice, B. Jutten, N. O. Kaakoush, K. Kaarniranta, A. Kaasik, T. Kabuta, B. Kaeffer, K. Kågedal, A. Kahana, S. Kajimura, O. Kakhlon, M. Kalia, D. V. Kalvakolanu, Y. Kamada, K. Kambas, V. O. Kaminskyy, H. H. Kampinga, M. Kandouz, C. Kang, R. Kang, T.-C. Kang, T. Kanki, T.-D. Kanneganti, H. Kanno, A. G. Kanthasamy, M. Kantorow, M. Kaparakis-Liaskos, O. Kapuy, V. Karantza, M. R. Karim, P. Karmakar, A. Kaser, S. Kaushik, T. Kawula, A. M. Kaynar, P.-Y. Ke, Z.-J. Ke, J. H. Kehrl, K. E. Keller, J. K. Kemper, A. K. Kenworthy, O. Kepp, A. Kern, S. Kesari, D. Kessel, R. Ketteler, I. do Carmo Kettelhut, B. Khambu, M. M. Khan, V. K. Khandelwal, S. Khare, J. G. Kiang, A. A. Kiger, A. Kihara, A. L. Kim, C. H. Kim, D. R. Kim, D.-H. Kim, E. K. Kim, H. Y. Kim, H.-R. Kim, J.-S. Kim, J. H. Kim, J. C. Kim, J. H. Kim, K. W. Kim, M. D. Kim, M.-M. Kim, P. K. Kim, S. W. Kim, S.-Y. Kim, Y.-S. Kim, Y. Kim, A. Kimchi, A. C. Kimmelman, T. Kimura, J. S. King, K. Kirkegaard, V. Kirkin, L. A. Kirshenbaum, S. Kishi, Y. Kitajima, K. Kitamoto, Y. Kitaoka, K. Kitazato, R. A. Kley, W. T. Klimecki, M. Klinkenberg, J. Klucken, H. Knævelsrud, E. Knecht, L. Knuppertz, J.-L. Ko, S. Kobayashi, J. C. Koch, C. Koechlin-Ramonatxo, U. Koenig, Y. H. Koh, K. Köhler, S. D. Kohlwein, M. Koike, M. Komatsu, E. Kominami, D. Kong, H. J. Kong, E. G. Konstantakou, B. T. Kopp, T. Korcsmaros, L. Korhonen, V. I. Korolchuk, N. V. Koshkina, Y. Kou, M. I. Koukourakis, C. Koumenis, A. L. Kovács, T. Kovács, W. J. Kovacs, D. Koya, C. Kraft, D. Krainc, H. Kramer, T. Kravic-Stevovic, W. Krek, C. Kretz-Remy, R. Krick, M. Krishnamurthy, J. Kriston-Vizi, G. Kroemer, M. C. Kruer, R. Kruger, N. T. Ktistakis, K. Kuchitsu, C. Kuhn, A. P. Kumar, A. Kumar, A. Kumar, D. Kumar, D. Kumar, R. Kumar, S. Kumar, M. Kundu, H.-J. Kung, A. Kuno, S.-H. Kuo, J. Kuret, T. Kurz, T. Kwok, T. K. Kwon, Y. T. Kwon, I. Kyrmizi, A. R. La Spada, F. Lafont, T. Lahm, A. Lakkaraju, T. Lam, T. Lamark, S. Lancel, T. H. Landowski, D. J. R. Lane, J. D. Lane, C. Lanzi, P. Lapaquette, L. R. Lapierre, J. Laporte, J. Laukkarinen, G. W. Laurie, S. Lavandero, L. Lavie, M. J. La Voie, B. Y. K. Law, H. K.-W. Law, K. B. Law, R. Layfield, P. A. Lazo, L. L. Cam, K. G. Le Roch, H. L. Stunff, V. Leardkamolkarn, M. Lecuit, B.-H. Lee, C.-H. Lee, E. F. Lee, G. M. Lee, H.-J. Lee, H. Lee, J. K. Lee, J. Lee, J.-H. Lee, J. H. Lee, M. Lee, M.-S. Lee, P. J. Lee, S. W. Lee, S.-J. Lee, S.-J. Lee, S. Y. Lee, S. H. Lee, S. S. Lee, S.-J. Lee, S. Lee, Y.-R. Lee, Y. J. Lee, Y. H. Lee, C. Leeuwenburgh, S. Lefort, R. Legouis, J. Lei, Q.-Y. Lei, D. A. Leib, G. Leibowitz, I. Lekli, S. D. Lemaire, J. J. Lemasters, M. K. Lemberg, A. Lemoine, S. Leng, G. Lenz, P. Lenzi, L. O. Lerman, D. L. Barbato, J. I.-J. Leu, H. Y. Leung, B. Levine, P. A. Lewis, F. Lezoualc'h, C. Li, F. Li, F.-J. Li, J. Li, K. Li, L. Li, M. Li, M. Li, Q. Li, R. Li, S. Li, W. Li, W. Li, X. Li, Y. Li, J. Lian, C. Liang, Q. Liang, Y. Liao, J. Liberal, P. P. Liberski, P. Lie, A. P. Lieberman, H. J. Lim, K.-L. Lim, K. Lim, R. T. Lima, C.-S. Lin, C.-F. Lin, F. Lin, F. Lin, F.-C. Lin, K. Lin, K.-H. Lin, P.-H. Lin, T. Lin, W.-W. Lin, Y.-S. Lin, Y. Lin, R. Linden, D. Lindholm, L. M. Lindqvist, P. Lingor, A. Linkermann, L. A. Liotta, M. M. Lipinski, V. A. Lira, M. P. Lisanti, P. B. Liton, B. Liu, C. Liu, C.-F. Liu, F. Liu, H.-J. Liu, J. Liu, J.-J. Liu, J.-L. Liu, K. Liu, L. Liu, L. Liu, Q. Liu, R.-Y. Liu, S. Liu, S. Liu, W. Liu, X.-D. Liu, X. Liu, X.-H. Liu, X. Liu, X. Liu, X. Liu, Y. Liu, Y. Liu, Z. Liu, Z. Liu, J. P. Liuzzi, G. Lizard, M. Ljujic, I. J. Lodhi, S. E. Logue, B. L. Lokeshwar, Y. C. Long, S. Lonial, B. Loos, C. López-Otín, C. López-Vicario, M. Lorente, P. L. Lorenzi, P. Lõrincz, M. Los, M. T. Lotze, P. E. Lovat, B. Lu, B. Lu, J. Lu, Q. Lu, S.-M. Lu, S. Lu, Y. Lu, F. Luciano, S. Luckhart, J. M. Lucocq, P. Ludovico, A. Lugea, N. W. Lukacs, J. J. Lum, A. H. Lund, H. Luo, J. Luo, S. Luo, C. Luparello, T. Lyons, J. Ma, Y. Ma, Y. Ma, Z. Ma, J. Machado, G. M. Machado-Santelli, F. Macian, G. C.MacIntosh, J. P. MacKeigan, K. F. Macleod, J. D. MacMicking, L. A. MacMillan-Crow, F. Madeo, M. Madesh, J. Madrigal-Matute, A. Maeda, T. Maeda, G. Maegawa, E. Maellaro, H. Maes, M. Magariños, K. Maiese, T. K. Maiti, L. Maiuri, M. C. Maiuri, C. G. Maki, R. Malli, W. Malorni, A. Maloyan, F. Mami-Chouaib, N. Man, J. D. Mancias, E.-M. Mandelkow, M. A. Mandell, A. A. Manfredi, S. N. Manié, C. Manzoni, K. Mao, Z. Mao, Z.-W. Mao, P. Marambaud, A. M. Marconi, Z. Marelja, G. Marfe, M. Margeta, E. Margittai, M. Mari, F. V. Mariani, C. Marin, S. Marinelli, G. Mariño, I. Markovic, R. Marquez, A. M. Martelli, S. Martens, K. R. Martin, S. J. Martin, S. Martin, M. A. Martin-Acebes, P. Martín-Sanz, C. Martinand-Mari, W. Martinet, J. Martinez, N. Martinez-Lopez, U. Martinez-Outschoorn, M. Martínez-Velázquez, M. Martinez-Vicente, W. K. Martins, H. Mashima, J. A. Mastrianni, G. Matarese, P. Matarrese, R. Mateo, S. Matoba, N. Matsumoto, T. Matsushita, A. Matsuura, T. Matsuzawa, M. P. Mattson, S. Matus, N. Maugeri, C. Mauvezin, A. Mayer, D. Maysinger, G. D. Mazzolini, M. K. McBrayer, K. M. Call, C. M. Cormick, G. M. McInerney, S. C. McIver, S. M. Kenna, J. J. McMahon, I. A. McNeish, F. Mechta-Grigoriou, J. P. Medema, D. L. Medina, K. Megyeri, M. Mehrpour, J. L. Mehta, Y. Mei, U.-C. Meier, A. J. Meijer, A. Meléndez, G. Melino, S. Melino, E. J. T. de Melo, M. A. Mena, M. D. Meneghini, J. A. Menendez, R. Menezes, L. Meng, L.-H. Meng, S. Meng, R. Menghini, A. S. Menko, R. F. Menna-Barreto, M. B. Menon, M. A. Meraz-Ríos, G. Merla, L. Merlini, A. M. Merlot, A. Meryk, S. Meschini, J. N. Meyer, M.-T. Mi, C.-Y. Miao, L. Micale, S. Michaeli, C. Michiels, A. R. Migliaccio, A. S. Mihailidou, D. Mijaljica, K. Mikoshiba, E. Milan, L. Miller-Fleming, G. B. Mills, I. G. Mills, G. Minakaki, B. A. Minassian, X.-F. Ming, F. Minibayeva, E. A. Minina, J. D. Mintern, S. Minucci, A. Miranda-Vizuete, C. H. Mitchell, S. Miyamoto, K. Miyazawa, N. Mizushima, K. Mnich, B. Mograbi, S. Mohseni, L. F. Moita, M. Molinari, M. Molinari, A. B. Møller, B. Mollereau, F. Mollinedo, M. Mongillo, M. M. Monick, S. Montagnaro, C. Montell, D. J. Moore, M. N. Moore, R. Mora-Rodriguez, P. I. Moreira, E. Morel, M. B. Morelli, S. Moreno, M. J. Morgan, A. Moris, Y. Moriyasu, J. L. Morrison, L. A. Morrison, E. Morselli, J. Moscat, P. L. Moseley, S. Mostowy, E. Motori, D. Mottet, J. C. Mottram, C. E.-H. Moussa, V. E. Mpakou, H. Mukhtar, J. M. M. Levy, S. Muller, R. Muñoz-Moreno, C. Muñoz-Pinedo, C. Münz, M. E. Murphy, J. T. Murray, A. Murthy, I. U. Mysorekar, I. R. Nabi, M. Nabissi, G. A. Nader, Y. Nagahara, Y. Nagai, K. Nagata, A. Nagelkerke, P. Nagy, S. R. Naidu, S. Nair, H. Nakano, H. Nakatogawa, M. Nanjundan, G. Napolitano, N. I. Naqvi, R. Nardacci, D. P. Narendra, M. Narita, A. C. Nascimbeni, R. Natarajan, L. C. Navegantes, S. T. Nawrocki, T. Y. Nazarko, V. Y. Nazarko, T. Neill, L. M. Neri, M. G. Netea, R. T. Netea-Maier, B. M. Neves, P. A. Ney, I. P. Nezis, H. T. Nguyen, H. P. Nguyen, A.-S. Nicot, H. Nilsen, P. Nilsson, M. Nishimura, I. Nishino, M. Niso-Santano, H. Niu, R. A. Nixon, V. C. Njar, T. Noda, A. A. Noegel, E. M. Nolte, E. Norberg, K. K. Norga, S. K. Noureini, S. Notomi, L. Notterpek, K. Nowikovsky, N. Nukina, T. Nürnberger, V. B. O'Donnell, T. O'Donovan, P. J. O'Dwyer, I. Oehme, C. L. Oeste, M. Ogawa, B. Ogretmen, Y. Ogura, Y. J. Oh, M. Ohmuraya, T. Ohshima, R. Ojha, K. Okamoto, T. Okazaki, F. J. Oliver, K. Ollinger, S. Olsson, D. P. Orban, P. Ordonez, I. Orhon, L. Orosz, E. J. O'Rourke, H. Orozco, A. L. Ortega, E. Ortona, L. D. Osellame, J. Oshima, S. Oshima, H. D. Osiewacz, T. Otomo, K. Otsu, J.-H. J. Ou, T. F. Outeiro, D.-Y. Ouyang, H. Ouyang, M. Overholtzer, M. A. Ozbun, P. H. Ozdinler, B. Ozpolat, C. Pacelli, P. Paganetti, G. Page, G. Pages, U. Pagnini, B. Pajak, S. C. Pak, K. Pakos-Zebrucka, N. Pakpour, Z. Palková, F. Palladino, K. Pallauf, N. Pallet, M. Palmieri, S. R. Paludan, C. Palumbo, S. Palumbo, O. Pampliega, H. Pan, W. Pan, T. Panaretakis, A. Pandey, A. Pantazopoulou, Z. Papackova, D. L. Papademetrio, I. Papassideri, A. Papini, N. Parajuli, J. Pardo, V. V. Parekh, G. Parenti, J.-I. Park, J. Park, O. K. Park, R. Parker, R. Parlato, J. B. Parys, K. R. Parzych, J.-M. Pasquet, B. Pasquier, K. B. Pasumarthi, D. Patschan, C. Patterson, S. Pattingre, S. Pattison, A. Pause, H. Pavenstädt, F. Pavone, Z. Pedrozo, F. J. Peña, M. A. Peñalva, M. Pende, J. Peng, F. Penna, J. M. Penninger, A. Pensalfini, S. Pepe, G. J. Pereira, P. C. Pereira, V. Pérez-dela Cruz, M. E. Pérez-Pérez, D. Pérez-Rodríguez, D. Pérez-Sala, C. Perier, A. Perl, D. H. Perlmutter, I. Perrotta, S. Pervaiz, M. Pesonen, J. E. Pessin, G. J. Peters, M. Petersen, I. Petrache, B. J. Petrof, G. Petrovski, J. M. Phang, M. Piacentini, M. Pierdominici, P. Pierre, V. Pierrefite-Carle, F. Pietrocola, F. X. Pimentel-Muiños, M. Pinar, B. Pineda, R. Pinkas-Kramarski, M. Pinti, P. Pinton, B. Piperdi, J. M. Piret, L. C. Platanias, H. W. Platta, E. D. Plowey, S. Pöggeler, M. Poirot, P. Polčic, A. Poletti, A. H. Poon, H. Popelka, B. Popova, I. Poprawa, S. M. Poulose, J. Poulton, S. K. Powers, T. Powers, M. Pozuelo-Rubio, K. Prak, R. Prange, M. Prescott, M. Priault, S. Prince, R. L. Proia, T. Proikas-Cezanne, H. Prokisch, V. J. Promponas, K. Przyklenk, R. Puertollano, S. Pugazhenthi, L. Puglielli, A. Pujol, J. Puyal, D. Pyeon, X. Qi, W.-B. Qian, Z.-H. Qin, Y. Qiu, Z. Qu, J. Quadrilatero, F. Quinn, N. Raben, H. Rabinowich, F. Radogna, M. J. Ragusa, M. Rahmani, K. Raina, S. Ramanadham, R. Ramesh, A. Rami, S. Randall-Demllo, F. Randow, H. Rao, V. A. Rao, B. B. Rasmussen, T. M. Rasse, E. A. Ratovitski, P.-E. Rautou, S. K. Ray, B. Razani, B. H. Reed, F. Reggiori, M. Rehm, A. S. Reichert, T. Rein, D. J. Reiner, E. Reits, J. Ren, X. Ren, M. Renna, J. E. Reusch, J. L. Revuelta, L. Reyes, A. R. Rezaie, R. I. Richards, D. R. Richardson, C. Richetta, M. A. Riehle, B. H. Rihn, Y. Rikihisa, B. E. Riley, G. Rimbach, M. R. Rippo, K. Ritis, F. Rizzi, E. Rizzo, P. J. Roach, J. Robbins, M. Roberge, G. Roca, M. C. Roccheri, S. Rocha, C. M. Rodrigues, C. I. Rodríguez, S. R. de Cordoba, N. Rodriguez-Muela, J. Roelofs, V. V. Rogov, T. T. Rohn, B. Rohrer, D. Romanelli,

L. Romani, P. S. Romano, M. I. G. Roncero, J. L. Rosa, A. Rosello, K. V. Rosen, P. Rosenstiel, M. Rost-Roszkowska, K. A. Roth, G. Roué, M. Rouis, K. M. Rouschop, D. T. Ruan, D. Ruano, D. C. Rubinsztein, E. B. Rucker III, A. Rudich, E. Rudolf, R. Rudolf, M. A. Ruegg, C. Ruiz-Roldan, A. A. Ruparelia, P. Rusmini, D. W. Russ, G. L. Russo, G. Russo, R. Russo, T. E. Rusten, V. Ryabovol, K. M. Ryan, S. W. Ryter, D. M. Sabatini, M. Sacher, C. Sachse, M. N. Sack, J. Sadoshima, P. Saftig, R. Sagi-Eisenberg, S. Sahni, P. Saikumar, T. Saito, T. Saitoh, K. Sakakura, M. Sakoh-Nakatogawa, Y. Sakuraba, M. Salazar-Roa, P. Salomoni, A. K. Saluja, P. M. Salvaterra, R. Salvioli, A. Samali, A. M. Sanchez, J. A. Sánchez-Alcázar, R. Sanchez-Prieto, M. Sandri, M. A. Sanjuan, S. Santaguida, L. Santambrogio, G. Santoni, C. N. D. Santos, S. Saran, M. Sardiello, G. Sargent, P. Sarkar, S. Sarkar, M. R. Sarrias, M. M. Sarwal, C. Sasakawa, M. Sasaki, M. Sass, K. Sato, M. Sato, J. Satriano, N. Savaraj, S. Saveljeva, L. Schaefer, U. E. Schaible, M. Scharl, H. M. Schatzl, R. Schekman, W. Scheper, A. Schiavi, H. M. Schipper, H. Schmeisser, J. Schmidt, I. Schmitz, B. E. Schneider, E. M. Schneider, J. L. Schneider, E. A. Schon, M. J. Schönenberger, A. H. Schönthal, D. F. Schorderet, B. Schröder, S. Schuck, R. J. Schulze, M. Schwarten, T. L. Schwarz, S. Sciarretta, K. Scotto, A. I. Scovassi, R. A. Screaton, M. Screen, H. Seca, S. Sedej, L. Segatori, N. Segev, P. O. Seglen, J. M. Seguí-Simarro, J. Segura-Aguilar, E. Seki, C. Sell, I. Seiliez, C. F. Semenkovich, G. L. Semenza, U. Sen, A. L. Serra, A. Serrano-Puebla, H. Sesaki, T. Setoguchi, C. Settembre, J. J. Shacka, A. N. Shajahan-Haq, I. M. Shapiro, S. Sharma, H. She, C.-K. J. Shen, C.-C. Shen, H.-M. Shen, S. Shen, W. Shen, R. Sheng, X. Sheng, Z.-H. Sheng, T. G. Shepherd, J. Shi, Q. Shi, Q. Shi, Y. Shi, S. Shibutani, K. Shibuya, Y. Shidoji, J.-J. Shieh, C.-M. Shih, Y. Shimada, S. Shimizu, D. W. Shin, M. L. Shinohara, M. Shintani, T. Shintani, T. Shioi, K. Shirabe, R. Shiri-Sverdlov, O. Shirihai, G. C. Shore, C.-W. Shu, D. Shukla, A. A. Sibirny, V. Sica, C. J. Sigurdson, E. M. Sigurdsson, P. S. Sijwali, B. Sikorska, W. A. Silveira, S. Silvente-Poirot, G. A. Silverman, J. Simak, T. Simmet, A. K. Simon, H.-U. Simon, C. Simone, M. Simons, A. Simonsen, R. Singh, S. V. Singh, S. K. Singh, D. Sinha, S. Sinha, F. A. Sinicrope, A. Sirko, K. Sirohi, B. J. Sishi, A. Sittler, P. M. Siu, E. Sivridis, A. Skwarska, R. Slack, I. Slaninová, N. Slavov, S. S. Smaili, K. S. Smalley, D. R. Smith, S. J. Soenen, S. A. Soleimanpour, A. Solhaug, K. Somasundaram, J. H. Son, A. Sonawane, C. Song, F. Song, H. K. Song, J.-X. Song, W. Song, K. Y. Soo, A. K. Sood, T. W. Soong, V. Soontornniyomkij, M. Sorice, F. Sotgia, D. R. Soto-Pantoja, A. Sotthibundhu, M. J. Sousa, H. P. Spaink, P. N. Span, A. Spang, J. D. Sparks, P. G. Speck, S. A. Spector, C. D. Spies, W. Springer, D. S. Clair, A. Stacchiotti, B. Staels, M. T. Stang, D. T. Starczynowski, P. Starokadomskyy, C. Steegborn, J. W. Steele, L. Stefanis, J. Steffan, C. M. Stellrecht, H. Stenmark, T. M. Stepkowski, S. T. Stern, C. Stevens, B. R. Stockwell, V. Stoka, Z. Storchova, B. Stork, V. Stratoulias, D. J. Stravopodis, P. Strnad, A. M. Strohecker, A.-L. Ström, P. Stromhaug, J. Stulik, Y.-X. Su, Z. Su, C. S. Subauste, S. Subramaniam, C. M. Sue, S. W. Suh, X. Sui, S. Sukseree, D. Sulzer, F.-L. Sun, Y. Sun, Y. Sun, Y. Sun, V. Sundaramoorthy, J. Sung, H. Suzuki, K. Suzuki, N. Suzuki, T. Suzuki, Y. J. Suzuki, M. S. Swanson, C. Swanton, K. Swärd, G. Swarup, S. T. Sweeney, P. W. Sylvester, Z. Szatmari, E. Szegezdi, P. W. Szlosarek, H. Taegtmeyer, M. Tafani, E. Taillebourg, S. W. Tait, K. Takacs-Vellai, Y. Takahashi, S. Takáts, G. Takemura, N. Takigawa, N. J. Talbot, E. Tamagno, J. Tamburini, C.-P. Tan, L. Tan, M. L. Tan, M. Tan, Y.-J. Tan, K. Tanaka, M. Tanaka, D. Tang, D. Tang, G. Tang, I. Tanida, K. Tanji, B. A. Tannous, J. A. Tapia, I. Tasset-Cuevas, M. Tatar, I. Tavassoly, N. Tavernarakis, A. Taylor, G. S. Taylor, G. A. Taylor, J. P. Taylor, M. J. Taylor, E. V. Tchetina, A. R. Tee, F. Teixeira-Clerc, S. Telang, T. Tencomnao, B.-B. Teng, R.-J. Teng, F. Terro, G. Tettamanti, A. L. Theiss, A. E. Theron, K. J. Thomas, M. P. Thomé, P. G. Thomes, A. Thorburn, J. Thorner, T. Thum, M. Thumm, T. L. Thurston, L. Tian, A. Till, J. P.-Y. Ting, V. I. Titorenko, L. Toker, S. Toldo, S. A. Tooze, I. Topisirovic, M. L. Torgersen, L. Torosantucci, A. Torriglia, M. R. Torrisi, C. Tournier, R. Towns, V. Trajkovic, L. H. Travassos, G. Triola, D. N. Tripathi, D. Trisciuoglio, R. Troncoso, I. P. Trougakos, A. C. Truttmann, K.-J. Tsai, M. P. Tschan, Y.-H. Tseng, T. Tsukuba, A. Tsung, A. S. Tsvetkov, S. Tu, H.-Y. Tuan, M. Tucci, D. A. Tumbarello, B. Turk, V. Turk, R. F. Turner, A. A. Tveita, S. C. Tyagi, M. Ubukata, Y. Uchiyama, A. Udelnow, T. Ueno, M. Umekawa, R. Umemiya-Shirafuji, B. R. Underwood, C. Ungermann, R. P. Ureshino, R. Ushioda, V. N. Uversky, N. L. Uzcátegui, T. Vaccari, M. I. Vaccaro, L. Váchová, H. Vakifahmetoglu-Norberg, R. Valdor, E. M. Valente, F. Vallette, A. M. Valverde, G. Van den Berghe, L. Van Den Bosch, G. R. van den Brink, F. G. van der Goot, I. J. van der Klei, L. J. van der Laan, W. G. van Doorn, M. van Egmond, K. L. van Golen, L. Van Kaer, M. van Lookeren Campagne, P. Vandenabeele, W. Vandenberghe, I. Vanhorebeek, I. Varela-Nieto, M. H. Vasconcelos, R. Vasko, D. G. Vavvas, I. Vega-Naredo, G. Velasco, A. D. Velentzas, P. D. Velentzas, T. Vellai, E. Vellenga, M. H. Vendelbo, K. Venkatachalam, N. Ventura, S. Ventura, P. S. Veras, M. Verdier, B. G. Vertessy, A. Viale, M. Vidal, H. L. A. Vieira, R. D. Vierstra, N. Vigneswaran, N. Vij, M. Vila, M. Villar, V. H. Villar, J. Villarroya, C. Vindis, G. Viola, M. T. Viscomi, G. Vitale, D. T. Vogl, O. V. Voitsekhovskaja, C. von Haefen, K. von Schwarzenberg, D. E. Voth, V. Vouret-Craviari, K. Vuori, J. M. Vyas, C. Waeber, C. L. Walker, M. J. Walker, J. Walter, L. Wan, X. Wan, B. Wang, C. Wang, C.-Y. Wang, C. Wang, C. Wang, C. Wang, D. Wang, F. Wang, F. Wang, G. Wang, H.-J. Wang, H. Wang, H.-G. Wang, H. Wang, H.-D. Wang, J. Wang, J. Wang, M. Wang, M.-Q. Wang, P.-Y. Wang, P. Wang, R. C. Wang, S. Wang, T.-F. Wang, X. Wang, X.-J. Wang, X.-W. Wang, X. Wang, X. Wang, Y. Wang, Y. Wang, Y. Wang, Y.-J. Wang, Y. Wang, Y. Wang, Y. T. Wang, Y. Wang, Z.-N. Wang, P. Wappner, C. Ward, D. M. Ward, G. Warnes, H. Watada, Y. Watanabe, K. Watase, T. E. Weaver, C. D. Weekes, J. Wei, T. Weide, C. C. Weihl, G. Weindl, S. N. Weis, L. Wen, X. Wen, Y. Wen, B. Westermann, C. M. Weyand, A. R. White, E. White, J. L. Whitton, A. J. Whitworth, J. Wiels, F. Wild, M. E. Wildenberg, T. Wileman, D. S. Wilkinson, S. Wilkinson, D. Willbold, C. Williams, K. Williams, P. R. Williamson, K. F. Winklhofer, S. S. Witkin, S. E. Wohlgemuth, T. Wollert, E. J. Wolvetang, E. Wong, G. W. Wong, R. W. Wong, V. K. W. Wong, E. A. Woodcock, K. L. Wright, C. Wu, D. Wu, G. S. Wu, J. Wu, J. Wu, M. Wu, M. Wu, S. Wu, W. K. Wu, Y. Wu, Z. Wu, C. P. Xavier, R. J. Xavier, G.-X. Xia, T. Xia, W. Xia, Y. Xia, H. Xiao, J. Xiao, S. Xiao, W. Xiao, C.-M. Xie, Z. Xie, Z. Xie, M. Xilouri, Y. Xiong, C. Xu, C. Xu, F. Xu, H. Xu, H. Xu, J. Xu, J. Xu, J. Xu, L. Xu, X. Xu, Y. Xu, Y. Xu, Z.-X. Xu, Z. Xu, Y. Xue, T. Yamada, A. Yamamoto, K. Yamanaka, S. Yamashina, S. Yamashiro, B. Yan, B. Yan, X. Yan, Z. Yan, Y. Yanagi, D.-S. Yang, J.-M. Yang, L. Yang, M. Yang, P.-M. Yang, P. Yang, Q. Yang, W. Yang, W. Y. Yang, X. Yang, Y. Yang, Y. Yang, Z. Yang, Z. Yang, M.-C. Yao, P. J. Yao, X. Yao, Z. Yao, Z. Yao, L. S. Yasui, M. Ye, B. Yedvobnick, B. Yeganeh, E. S. Yeh, P. L. Yeyati, F. Yi, L. Yi, X.-M. Yin, C. K. Yip, Y.-M. Yoo, Y. H. Yoo, S.-Y. Yoon, K.-I. Yoshida, T. Yoshimori, K. H. Young, H. Yu, J. J. Yu, J.-T. Yu, J. Yu, L. Yu, W. H. Yu, X.-F. Yu, Z. Yu, J. Yuan, Z.-M. Yuan, B. Y. Yue, J. Yue, Z. Yue, D. N. Zacks, E. Zacksenhaus, N. Zaffaroni, T. Zaglia, Z. Zakeri, V. Zecchini, J. Zeng, M. Zeng, Q. Zeng, A. S. Zervos, D. D. Zhang, F. Zhang, G. Zhang, G.-C. Zhang, H. Zhang, H. Zhang, H. Zhang, H. Zhang, J. Zhang, J. Zhang, J. Zhang, J. Zhang, J.-P. Zhang, L. Zhang, L. Zhang, L. Zhang, L. Zhang, M.-Y. Zhang, X. Zhang, X. D. Zhang, Y. Zhang, Y. Zhang, Y. Zhang, Y. Zhang, Y. Zhang, M. Zhao, W.-L. Zhao, X. Zhao, Y. G. Zhao, Y. Zhao, Y. Zhao, Y.-X. Zhao, Z. Zhao, Z. J. Zhao, D. Zheng, X.-L. Zheng, X. Zheng, B. Zhivotovsky, Q. Zhong, G.-Z. Zhou, G. Zhou, H. Zhou, S.-F. Zhou, X.-J. Zhou, H. Zhu, H. Zhu, W.-G. Zhu, W. Zhu, X.-F. Zhu, Y. Zhu, S.-M. Zhuang, X. Zhuang, E. Ziparo, C. E. Zois, T. Zoladek, W.-X. Zong, A. Zorzano, S. M. Zughaier, Guidelines for the use and interpretation of assays for monitoring autophagy (3rd edition). *Autophagy* **12**, 1–222 (2016).

39. I. Grigoriev, D. Splinter, N. Keijzer, P. S. Wulf, J. Demmers, T. Ohtsuka, M. Modesti, I. V. Maly, F. Grosveld, C. C. Hoogenraad, A. Akhmanova, Rab6 regulates transport and targeting of exocytotic carriers. *Dev. Cell* **13**, 305–314 (2007).
40. M. Ostrowski, N. B. Carmo, S. Krumeich, I. Fanget, G. Raposo, A. Savina, C. F. Moita, K. Schauer, A. N. Hume, R. P. Freitas, B. Goud, P. Benaroch, N. Hacohen, M. Fukuda, C. Desnos, M. C. Seabra, F. Darchen, S. Amigorena, L. F. Moita, C. Thery, Rab27a and Rab27b control different steps of the exosome secretion pathway. *Nat. Cell Biol.* **12**, 19–30 (2010).
41. I. Jordens, M. Fernandez-Borja, M. Marsman, S. Dusseljee, L. Janssen, J. Calafat, H. Janssen, R. Wubbolts, J. Neefjes, The Rab7 effector protein RILP controls lysosomal transport by inducing the recruitment of dynein-dynactin motors. *Curr. Biol.* **11**, 1680–1685 (2001).
42. F. Guerra, C. Bucci, Multiple roles of the small GTPase Rab7. *Cell* **5**, 34 (2016).
43. M. S. Robinson, D. A. Sahlender, S. D. Foster, Rapid inactivation of proteins by rapamycin-induced rerouting to mitochondria. *Dev. Cell* **18**, 324–331 (2010).
44. K. L. Schalinske, K. P. Blemings, D. W. Steffen, O. S. Chen, R. S. Eisenstein, Iron regulatory protein 1 is not required for the modulation of ferritin and transferrin receptor expression by iron in a murine pro-B lymphocyte cell line. *Proc. Natl. Acad. Sci. U.S.A.* **94**, 10681–10686 (1997).
45. R. Y. Chan, C. Seiser, H. M. Schulman, L. C. Kühn, P. Ponka, Regulation of transferrin receptor mRNA expression. Distinct regulatory features in erythroid cells. *Eur. J. Biochem.* **220**, 683–692 (1994).
46. H. Farhan, Systems biology of the secretory pathway: What have we learned so far? *Biol. Cell* **107**, 205–217 (2015).
47. S. Shibata, T. Kawanai, T. Hara, A. Yamamoto, T. Chaya, Y. Tokuhara, C. Tsuji, M. Sakai, T. Tachibana, S. Inagaki, ARHGEF10 directs the localization of Rab8 to Rab6-positive executive vesicles. *J. Cell Sci.* **129**, 3620–3634 (2016).
48. T. Tsuboi, M. Fukuda, Rab3A and Rab27A cooperatively regulate the docking step of dense-core vesicle exocytosis in PC12 cells. *J. Cell Sci.* **119**, 2196–2203 (2006).
49. S. K. G. Gadila, K. Kim, Cargo trafficking from the trans-Golgi network towards the endosome. *Biol. Cell* **108**, 205–218 (2016).
50. I. Jordens, W. Westbroek, M. Marsman, N. Rocha, M. Mommaas, M. Huizing, J. Lambert, J. M. Naeyaert, J. Neefjes, Rab7 and Rab27a control two motor protein activities involved in melanosomal transport. *Pigment Cell Res.* **19**, 412–423 (2006).
51. A. Jimenez-Orgaz, A. Kvainickas, H. Nägele, J. Denner, S. Eimer, J. Dengjel, F. Steinberg, Control of RAB7 activity and localization through the retromer-TBC1D5 complex enables RAB7-dependent mitophagy. *EMBO J.* **37**, 235–254 (2018).
52. F. A. Ran, P. D. Hsu, J. Wright, V. Agarwala, D. A. Scott, F. Zhang, Genome engineering using the CRISPR-Cas9 system. *Nat. Protoc.* **8**, 2281–2308 (2013).
53. J. Cox, M. Y. Hein, C. A. Luber, I. Paron, N. Nagaraj, M. Mann, Accurate proteome-wide label-free quantification by delayed normalization and maximal peptide ratio extraction, termed MaxLFQ. *Mol. Cell. Proteomics* **13**, 2513–2526 (2014).
54. C. Carapito, A. Burel, P. Guterl, A. Walter, F. Varrier, F. Bertile, A. Van Dorsselaer, MSDA, a proteomics software suite for in-depth Mass Spectrometry Data Analysis using grid computing. *Proteomics* **14**, 1014–1019 (2014).

55. S. Wieczorek, F. Combes, C. Lazar, Q. Giai Gianetto, L. Gatto, A. Dorffer, A.-M. Hesse, Y. Couté, M. Ferro, C. Bruley, T. Burger, DAPAR & ProStaR: Software to perform statistical analyses in quantitative discovery proteomics. *Bioinformatics* **33**, 135–136 (2017).
56. J. A. Vizcaíno, E. W. Deutsch, R. Wang, A. Csordas, F. Reisinger, D. Ríos, J. A. Dianes, Z. Sun, T. Farrah, N. Bandeira, P.-A. Binz, I. Xenarios, M. Eisenacher, G. Mayer, L. Gatto, A. Campos, R. J. Chalkley, H.-J. Kraus, J. P. Albar, S. Martinez-Bartolomé, R. Apweiler, G. S. Omenn, L. Martens, A. R. Jones, H. Hermjakob, ProteomeXchange provides globally coordinated proteomics data submission and dissemination. *Nat. Biotechnol.* **32**, 223–226 (2014).
57. J. A. Vizcaíno, A. Csordas, N. del-Toro, J. A. Dianes, J. Griss, I. Lavidas, G. Mayer, Y. Perez-Riverol, F. Reisinger, T. Ternent, Q.-W. Xu, R. Wang, H. Hermjakob, 2016 update of the PRIDE database and its related tools. *Nucleic Acids Res.* **44**, D447–D456 (2016).
58. J. Schindelin, I. Arganda-Carreras, E. Frise, V. Kaynig, M. Longair, T. Pietzsch, S. Preibisch, C. Rueden, S. Saalfeld, B. Schmid, J.-Y. Tinevez, D. J. White, V. Hartenstein, K. Eliceiri, P. Tomancak, A. Cardona, Fiji: An open-source platform for biological-image analysis. *Nat. Methods* **9**, 676–682 (2012).

Acknowledgments: We acknowledge the imaging facility MRI, member of the National Infrastructure France-BioImaging. We thank L. Espert and colleagues for helpful discussions and sharing reagents related to autophagy. We thank M. Bonazzi and colleagues for advice and reagents related to Rab7. We thank T. Kirchhausen for supportive discussions. GFP-Rab7A was a gift from G. Voeltz (Addgene plasmid #61803), and EGFP-Rab7A T22N was a gift from Q. Zhong (Addgene plasmid #28048). **Funding:** MS-related work was financially supported by the "Agence Nationale de la Recherche" (ANR) and the French Proteomic Infrastructure (ProFI; ANR-10-INBS-08-03). This work was supported by the Ministry of Science and Technology of the People's Republic of China (2018YFA0507101) and the National Natural Science Foundation of China (31770900). Laboratory work in the laboratory of F.P. is supported by the Institut Curie, the Centre National de la Recherche Scientifique, the Labex CelTisPhyBio (ANR-10-LABX-62-IBEID and ANR-10-IDEX-0001-02 PSL), the Agence Nationale de la Recherche (ANR-17-CE13-0021-02, ANR-17-CE15-0025-02), and La Fondation pour la Recherche Médicale (EQU201903007925). This work was supported by the IdEx Université de Strasbourg, the Agence Nationale de la Recherche (ANR-18-CE13-0003-01), and an ATIP-AVENIR starting grant to R.G. **Author contributions:** M.S.D. and R.G. conceived the experiments. M.S.D., I.C., C.D., V.L., and R.G. generated and characterized the TfR-eRUSH cell line. M.S.D., I.C., and R.G. performed flow cytometry. I.C. conducted the siRNA-based assays. M.S.D. and R.G. performed the microscopy analyses. F.D. and A.H. conducted MS, and F.D., S.C., C.C., and R.G. analyzed the proteomics data. E.S. generated constructs for imaging. G.B. and F.P. provided technical and conceptual support. R.G. and M.S.D. wrote the manuscript. R.G., M.S.D., C.D., F.D., and C.C. edited and commented on the manuscript. **Competing interests:** The authors declare that they have no competing interests. **Data and materials availability:** All data needed to evaluate the conclusions in the paper are present in the paper and/or the Supplementary Materials. The MS proteomics data have been deposited in the ProteomeXchange Consortium database with the identifier PXD010576. Additional data related to this paper may be requested from the authors.

Submitted 5 January 2020
Accepted 18 November 2020
Published 8 January 2021
10.1126/sciadv.aba7803

Citation: M. S. Deffieu, I. Cesonyte, F. Delalande, G. Boncompain, C. Dorobantu, E. Song, V. Lucansky, A. Hirschler, S. Cianferani, F. Perez, C. Carapito, R. Gaudin, Rab7-harboring vesicles are carriers of the transferrin receptor through the biosynthetic secretory pathway. *Sci. Adv.* **7**, eaba7803 (2021).

Science Advances

Rab7-harboring vesicles are carriers of the transferrin receptor through the biosynthetic secretory pathway

Maika S. Deffieu, Ieva Cesonyte, François Delalande, Gaelle Boncompain, Cristina Dorobantu, Eli Song, Vincent Lucansky, Aurélie Hirschler, Sarah Cianferani, Franck Perez, Christine Carapito and Raphael Gaudin

Sci Adv **7** (2), eaba7803.
DOI: 10.1126/sciadv.aba7803

Science Advances (ISSN 2375-2548) is published by the American Association for the Advancement of Science, 1200 New York Avenue NW, Washington, DC 20005. The title *Science Advances* is a registered trademark of AAAS.